NASA TM X-596

NASA TM X-596

TECHNICAL MEMORANDUM

X-596

HEAT-TRANSFER MEASUREMENTS IN REGIONS OF FLOW SEPARATION AND REATTACHMENT ON TWO AXISYMMETRIC MODELS AT MACH NUMBERS FROM 2.65 TO 4.50

By Robert L. Stallings, Jr., Ward F. Hodge, and Paige B. Burbank

Langley Research Center
Langley Air Force Base, Va.

[redacted]

NATIONAL AERONAUTICS AND SPACE ADMINISTRATION

WASHINGTON

October 1961

[redacted]

NATIONAL AERONAUTICS AND SPACE ADMINISTRATION

TECHNICAL MEMORANDUM X-596

HEAT-TRANSFER MEASUREMENTS IN REGIONS OF FLOW SEPARATION AND REATTACHMENT ON TWO AXISYMMETRIC MODELS AT MACH NUMBERS FROM 2.65 TO 4.50* **

By Robert L. Stallings, Jr., Ward F. Hodge, and Paige B. Burbank

SUMMARY

Heat-transfer coefficients on two axisymmetric models having downstream facing steps were determined in the Langley Unitary Plan wind tunnel. One model, denoted as the stepped-cylinder model, consists of a truncated conical nose with a base radius larger than the cylindrical afterbody. The second model duplicates the downstream facing step at the juncture of the fourth and fifth stages of an NASA five-stage research vehicle.

The stepped-cylinder model with artificial transition was tested at Mach numbers of 2.65 and 3.51, Reynolds numbers per foot from 0.8×10^6 to 3.1×10^6, and angles of attack from 0° to 20°. At all angles of attack the heating rates on the nose in and downstream of the region of reattachment were predicted by turbulent cone theory based on the local Mach number and the local Reynolds number using a distance measured from the stagnation point on the front face. At an angle of attack of 0° the measured heat-transfer rates downstream of the region of separation at the rearward facing step were in good agreement with turbulent flat-plate theory based on local conditions and a boundary layer originating at the region of reattachment. The maximum heat-transfer coefficient in the reattachment region along the windward meridian of the cylinder at an angle of attack of 20° was 115 percent of the measured stagnation-point value at an angle of attack of 0°.

Author

*The contribution of Robert L. Stallings, Jr., to the subject paper was in part presented as a thesis entitled "An Investigation of the Aerodynamic Heating Rates in Regions of Flow Reattachment on Two Axisymmetric Configurations," which was offered in partial fulfillment of the requirements for the degree of Master of Science in Aeronautical Engineering, Virginia Polytechnic Institute, Blacksburg, Virginia, May 1961.

**Title, Unclassified.

The measured heating rates along the windward meridian downstream of the region of reattachment at angles of attack greater than 0° were in good agreement with turbulent infinite-swept-cylinder theory.

The five-stage research vehicle model was tested at Mach numbers of 3.51 and 4.50, Reynolds numbers per foot from 2.8×10^6 to 4.5×10^6, and an angle of attack of 0°. The measured values downstream of the rearward facing step were in good agreement with turbulent flat-plate theory evaluated at local conditions and a local Reynolds number based on the axial length from the forward stagnation point.

INTRODUCTION

Wind-tunnel tests of the Project Mercury reentry configuration have indicated heat-transfer rates in the flow reattachment regions on the rearward part of the spacecraft to be of the same order of magnitude as those on the stagnation point of the ablation shield. (See ref. 1.) A survey of the literature indicated that the limited amount of existing information pertaining to the boundary-layer properties associated with the flow reattachment region downstream of a rearward facing step is primarily concerned with a two-dimensional-flow field, for example, references 2, 3, and 4. Therefore, an experimental program at the Langley Unitary Plan wind tunnel is now in progress to evaluate the effects of nose shape, model attitude, and free-stream variables on the aerodynamic heating associated with the reattachment region on axisymmetric bodies. In order to expedite publication of the phase of the program for which experimental tests are completed, only two models will be discussed in this paper. One model, denoted as the stepped-cylinder model, consists of a truncated-cone nose section and a cylindrical afterbody, the radius of the base of the nose being larger than the radius of the cylinder and thus forming a downstream facing step at the nose-afterbody juncture. The second model duplicates the fairing of the fourth and fifth stages of an NASA five-stage research vehicle. This model has a downstream facing step at the juncture of the fourth and fifth stages, and it was speculated that, if reattachment occurred as in reference 1, the resultant high heating rates on a magnesium stage fairing could be the reason for previous unexplained vehicle failures.

The stepped-cylinder model was tested at angles of attack from 0° to 20° at Mach numbers of 2.65 and 3.51; the five-stage research vehicle model was tested at an angle of attack of 0° at Mach numbers of 3.51 and 4.50.

SYMBOLS

C_p	pressure coefficient, $\frac{p_l - p_\infty}{q_\infty}$
c	specific heat of model skin, Btu/lb-^oR
h	heat-transfer coefficient, Btu/sec-ft^2-^oR
M	Mach number
N_{St}	Stanton number
p	pressure, lb/sq ft
$p_{t,2}$	stagnation pressure behind normal shock, lb/sq ft
q	dynamic pressure, lb/sq ft
r	flat-face-nose radius of stepped-cylinder model, 0.073 ft
R	free-stream Reynolds number per foot
t	time, sec
T_t	stagnation temperature, ^oR
T_w	wall temperature, ^oR
$T_{w,e}$	measured wall equilibrium temperature, ^oR
w	weight of model skin per unit area, lb/sq ft
x_1, x_2, x_3	surface coordinates of stepped-cylinder model along flat-face nose, conical frustum, and cylindrical afterbody (defined in fig. 1), in.
y	step height of stepped-cylinder model (defined in fig. 1), 0.05 ft
α	angle of attack, deg
γ	ratio of specific heats, 1.4 for air
ϵ	emissivity

σ Stefan-Boltzmann constant, 0.484×10^{-12}, Btu/sec-ft^2-$^\circ$R^4

ϕ meridian angle, measured in plane normal to axis of symmetry, deg

Subscripts:

i indices of summation

l local conditions at outer edge of boundary layer

s conditions along stagnation line of infinite swept cylinder

t stagnation

0,1,2,3,...,n time sequence

∞ free-stream conditions

DESCRIPTION OF MODELS

The construction of the stepped-cylinder model, as illustrated in figure 1, consisted of a truncated conical nose having a 20° half-angle and a base radius 0.6 inch larger than the radius of a cylindrical afterbody. The model was constructed with interchangeable cylinders to facilitate detailed measurements of both pressure and heat-transfer coefficients. Evaluation of the heat-transfer coefficients from transient-wall-temperature measurements necessitates thin-walled construction; therefore, the nose section and the cylinder instrumented with thermocouples were constructed by spinning and rolling a 0.030-inch Inconel sheet on form mandrels. Heat losses due to internal conduction, internal convection, and external radiation were minimized by using bulkheads constructed of Transite insulating material relieved in the vicinity of the thermocouples, by venting the shell interior to free-stream static pressure, and by polishing the model to a 10-microinch finish. Pressure measurements were obtained on the thin-walled nose section and the thick-walled cylinder illustrated in figure 1(a). Photographs of both the pressure and heat-transfer configurations are shown in figure 2. The heat-transfer configuration was sprayed with an acrylic plastic to decrease the surface luster for photographing.

A second model consisted of the actual outer shell of the fifth stage and a simulated portion of the fourth stage of an NASA five-stage research vehicle. As illustrated in figures 3 and 4, a downstream step exists between the fourth and fifth stages of this model. The model was

constructed as illustrated in figure 3 in the same manner as the stepped-cylinder model to minimize heat losses due to internal conduction, internal convection, and external radiation. In order to minimize lateral deflections of the model during the test, a thick-walled tube was used for internal support with the thin-walled model components attached to it by several flange connections.

INSTRUMENTATION

The stepped-cylinder model was instrumented with sixty No. 30 gage iron-constantan thermocouples and twenty-one static-pressure orifices having 0.035-inch inside diameters. Two stagnation-temperature probes were mounted on the sting behind the model at deflection angles of 0° and 10° to the model center line. The location of the thermocouples and pressure orifices as shown in figure 1 is defined by an angle ϕ and surface coordinates x_1, x_2, x_3 with origins at the stagnation point on the flat front face, at the juncture of the flat front face and the conical nose, and at the juncture of the conical nose and the cylinder, respectively. The angle ϕ is oriented so that when $0^\circ \leq \phi \leq 90^\circ$ the instrumentation is on the windward half of the model, and when $90^\circ \leq \phi \leq 180^\circ$ the instrumentation is on the leeward half of the model. The local wall thickness is also presented in figure 1 for each thermocouple location. Each thermocouple output was recorded on a multichannel sequential analog to digital conversion system discussed in reference 5.

The local total pressure outside the boundary layer was determined from measurements taken with a two-tube rake located near the base of the nose section and a six-tube rake located at two axial stations on the cylinder. These rakes are shown in figure 1. The local pressures were measured by electrical transducers and each electrical output was recorded on digital self-balancing potentiometers.

The five-stage research vehicle model was instrumented with 57 iron-constantan thermocouples. The location of the thermocouples and the local wall thicknesses are shown in figure 3. Two stagnation-temperature probes were mounted at the base of the model in line with the two rows of thermocouples. The local free-stream Mach number at the base of the simulated fourth stage was determined by static- and total-pressure measurements.

The tunnel free-stream static and stagnation pressures were measured on precision mercury manometers.

APPARATUS AND TEST CONDITIONS

This investigation was conducted in the high Mach number test section of the Langley Unitary Plan wind tunnel described in reference 6. This variable-pressure, continuous-flow tunnel has an asymmetrical sliding-block nozzle that permits a continuous variation in the test-section Mach number from 2.3 to 4.65. The deviation in Mach number over the entire 4- by 4-foot test section for Mach numbers of 2.65, 3.51, and 4.50 is ±0.03, ±0.05, and ±0.06, respectively.

Both stepped-cylinder configurations had artificial transition in the form of No. 60 carborundum grains located on the conical nose as illustrated in figure 1.

Heat-transfer coefficients for both models and pressure coefficients for the stepped-cylinder model were determined for the following test conditions:

Models	Test	α, deg	Mach number	Stagnation pressure (nominal), lb/sq in. abs
Stepped cylinder	Static pressure	0, 5, 10, 15, 20	2.65	20
Stepped cylinder	Total pressure	0, 5, 10, 15, 20	2.65	20
Stepped cylinder	Heat transfer	0, 5, 10, 15, 20	2.65	20
Stepped cylinder	Heat transfer	0, 5, 10, 15, 20	3.51	35
Stepped cylinder	Heat transfer	0, 10	3.51	10
Five-stage research vehicle	Heat transfer	0	3.51	56, 35
Five-stage research vehicle	Heat transfer	0	4.50	85, 60

The static- and total-pressure tests were conducted separately to avoid interference effects and, due to limited tunnel time, pressure measurements were not obtained at $M = 3.51$.

METHOD OF HEAT-TRANSFER-DATA REDUCTION

The heat-transfer coefficients were obtained from transient-skin-temperature measurements resulting from a stepwise increase in stagnation temperature as discussed in reference 5. The following relation, which assumes constant temperature through the skin, negligible lateral heat flow, negligible heat flow to the model interior, and no heat losses due to radiation, was used:

$$h = \frac{wc\left(\frac{dT_w}{dt}\right)}{T_{w,e} - T_w}$$

This equation as shown in reference 5 can be written in the following form for complete machine calculation:

$$h = \frac{wc\left(T_{w,n} - T_{w,0}\right)}{\frac{T_{w,e}}{T_t}\sum_{0}^{n-1}\left(T_t\right)_i \Delta t - \sum_{0}^{n-1}\left(T_w\right)_i \Delta t} \qquad (1)$$

The summations are evaluated over increments of time according to the trapezoidal rule

$$\sum_{0}^{n-1}(T)_i \Delta t = \Delta t\left(\frac{1}{2}T_0 + \frac{1}{2}T_n + T_1 + T_2 + \cdots + T_{n-1}\right)$$

and the ratio $T_{w,e}/T_t$ is experimentally determined.

The magnitude of the lateral heat flow for a thin-skin model as discussed in reference 1 is negligible. The heat flow caused by radiation is dependent upon the term $\sigma\epsilon\left(T_w^4 - T_a^4\right)$, where T_a is the tunnel wall temperature, and this term is negligible.

ACCURACY

The accuracy of the temperature measurements including recorder resolution, thermocouple-wire calibration, and cold junctions is $\pm 2^{\circ}$ F; however, this error will occur in temperature level rather than in random temperature fluctuations. A temperature error of $\pm 2^{\circ}$ F could result in ratios of equilibrium temperature to stagnation temperature $T_{w,e}/T_t$ greater than 1 in stagnation regions of the model. Also, as discussed in reference 5, in regions of low heat transfer (h less than 0.001), the ratio $T_{w,e}/T_t$ may be questionable, because the wall temperature may not have reached equilibrium from the preceding test point.

An estimation of the accuracy of heat-transfer measurements in the Langley Unitary Plan wind tunnel has been determined by the repeatability of data in the tests discussed in reference 1. The accuracy is dependent upon the magnitude of the heat-transfer coefficient. For $h > 0.0150$, the accuracy is within 10 percent; for $0.0010 < h < 0.0150$, within 15 percent; and for $h < 0.0010$, within 20 percent. Although $h < 0.0010$ is within the accuracy of data reduction, no significance is attached to the magnitude of h other than to indicate the low-heat-transfer regions.

The accuracy of the precision manometers is within 0.5 lb/sq ft. Therefore, the accuracy of the system is limited to that of the electrical transducer which is 0.5 percent of full-scale deflection. The maximum possible error in the pressure coefficient resulting from the inaccuracy of the electrical transducer is 0.0165.

RESULTS AND DISCUSSION

Schlieren pictures taken of both the stepped-cylinder model and the five-stage research vehicle model and shadowgraph photographs of the stepped-cylinder model are presented in figures 5, 6, and 7. Complete lists of the pressure data obtained on the stepped-cylinder model and the heat-transfer data obtained on both models throughout the range of test variables are presented in tables I to IV.

Pressure Distribution for Stepped-Cylinder Model

Conical nose.- The local-pressure-coefficient distribution over the conical segment of the nose is presented in figure 8(a) for $M = 2.65$, $R = 3.1 \times 10^6$, and angles of attack of 0°, 10°, and 20°. The approximate location of the flow reattachment points as determined from shadowgraphs

is indicated by the solid symbols on the abscissa scale. Due to the lack of instrumentation in the separated region, the extent of the effects of separation on the pressure distribution cannot be specified; however, at $\alpha = 0^\circ$ these effects occur over a surface length approximately twice that of the visible separation on the shadowgraphs. This same trend will be shown subsequently in the heat-transfer-coefficient distribution. In the region of uniform pressure downstream of the effect of reattachment, the pressure coefficients are approximately 15 percent less than the theoretical cone values determined from reference 7. A similar disagreement between experimental and theoretical values was obtained on a blunted conical nose at $M = 3.55$ in reference 8. Increasing the angle of attack to 10° resulted in an increase in the pressure coefficients and a decrease in the extent of separation effects. As a crude approximation, the elevated pressure coefficients at this angle of attack were approximated by a 30° cone at an angle of attack of 0°. This approximation overpredicted the experimental values by approximately 10 percent. At an angle of attack of 20°, this prediction for a 40° cone at $\alpha = 0^\circ$ was approximately 3 percent greater than the experimental values. Since local pressures are necessary in the analysis of heat-transfer investigations and experimental pressures were not obtained at $M = 3.51$ for this investigation, they were approximated by an equivalent cone at an angle of attack of 0° as a result of the agreement obtained with experimental and theoretical values at $M = 2.65$.

L 1503

Cylindrical afterbody.- The local-pressure-coefficient distribution over the cylindrical afterbody is shown in figure 8(b) for $M = 2.65$, $R = 3.1 \times 10^6$, and angles of attack of 0°, 10°, and 20°. The approximate location of the flow reattachment points on the cylinder as determined from shadowgraphs is represented by the solid symbols on the abscissa scale. At an angle of attack of 0°, the effect of the separated region on the pressure coefficients is similar to the results obtained on the conical nose and extends to approximately 1.5 times the measured length of separation. Downstream of the region affected by separation, the local pressure returns to approximately the free-stream value, resulting in pressure coefficients of zero magnitude. The local Mach numbers on the cylinder as determined from measured local static and total pressures are approximately constant at a value of 2.1.

At angles of attack of both 10° and 20°, the experimental pressure coefficients downstream of the effects of separation are in good agreement with predicted values from the following equation (ref. 9):

$$\frac{p_s}{p_{t,2}} = \sin^2\alpha + \left[\frac{\left(\frac{2\gamma M^2}{\gamma+1} - \frac{\gamma-1}{\gamma+1}\right)^{\frac{1}{\gamma-1}}}{\left(\frac{\gamma+1}{2}M^2\right)^{\frac{\gamma}{\gamma-1}}}\right]\cos^2\alpha \qquad (2)$$

This equation defines the stagnation-pressure ratio along the stagnation line of an infinite swept cylinder evaluated at the free-stream conditions. This agreement was rather surprising as it indicates that the end effects of this configuration on the inviscid flow field outside the boundary layer on the windward side of the cylinder downstream of reattachment are small.

Heat-Transfer Distribution for Stepped-Cylinder Model

Nose section.- The experimental distribution of h on the flat front face portion of the nose is in good agreement with the experimental distributions presented in reference 10 and hence will not be discussed herein. The measured distribution of h on the conical portion of the nose is presented in figure 9 for Mach numbers of 2.65 and 3.51, Reynolds numbers of 0.8×10^6, 2.5×10^6, and 2.8×10^6, and angles of attack of 0°, 10°, and 20°. At $M = 2.65$ and an angle of attack of 0° (fig. 9(a)), the measured heat-transfer coefficients associated with the separated region at the corner (formed at the intersection of the front face with the conical side) extend to approximately twice the measured distance of separation. The maximum measured h in the region of reattachment is approximately the same magnitude as the measured h at the stagnation point on the front face. However, the experimental values in and downstream of the region of reattachment are in fair agreement with turbulent conical theory (ref. 11) using measured static pressures and wall temperatures, the total pressure behind a normal shock at free-stream Mach number, and a surface length measured from the stagnation point on the flat front face. The movement of the stagnation point with α was determined from reference 10. Although the maximum heat-transfer coefficients in the reattachment regions at angles of attack of 10° and 20° are approximately 170 percent and 200 percent, respectively, of the measured stagnation-point value at an angle of attack of 0°, the evaluated distribution of h is predicted by the turbulent cone theory. At an angle of attack of 20°, the predicted h is low; closer agreement of theory with experiment has been obtained (although not shown in fig. 9(a)) with a Reynolds number based on the surface distance from the juncture of the flat face and the conical surface.

The heat-transfer-coefficient distribution for $M = 3.51$ and a Reynolds number of 2.8×10^6 are shown in figure 9(b). The theoretical values of h were computed by the method outlined for $M = 2.65$, except that the local static pressures were determined from the pressure coefficients of the equivalent conical flow, as mentioned in the pressure analysis, and the total pressure was assumed to correspond to that behind a normal shock at the free-stream Mach number. At an angle of attack of 0°, the experimental values of h at the forward thermocouples are of the same magnitude as predicted by laminar theory; however, at the

rearward thermocouples the experimental values approach the turbulent theoretical values, thus indicating a gradual transition from laminar to turbulent flow. The distribution of h for a Mach number of 3.51 at the angles of attack other than 0° is very similar to that measured at a Mach number of 2.65; that is, the highest heating occurs in the reattachment region and these maximum values increase with increasing angle of attack. At angles of attack of 10° and 20°, the maximum heat-transfer coefficients were approximately 120 percent and 175 percent of the stagnation-point value at an angle of attack of 0°; however, these maximum values are approximated by the turbulent cone theory.

The effect of decreasing the Reynolds number from 2.8×10^6 to 0.8×10^6 at $M = 3.51$ and at angles of attack of 0° and 10° is also shown in figure 9(b). The high heating associated with reattachment as previously noted does not occur at the low Reynolds number at either angle of attack. The magnitude of the heating rates at the low Reynolds number is approximately 60 percent of the turbulent theory at both values of α; however, the laminar conical theory (ref. 11), based on the same conditions as the turbulent theory, is in very good agreement with the experimental data.

A comparison of the heating rates in the reattachment region on the conical nose section associated with a turbulent boundary layer with those associated with a laminar boundary layer indicates that the comparatively high heat rates in this reattachment region are primarily a function of the nature of the boundary layer rather than the reattachment mechanism in itself and that, furthermore, these heating rates can be estimated by existing theories provided the local conditions and the nature of the boundary layer are known.

Cylindrical afterbody.- The effect of angle of attack, Mach number, and Reynolds number on the heat-transfer-coefficient distribution along the windward meridian of the cylindrical afterbody is presented in figure 10. For purposes of comparison, the measured heat-transfer coefficient at the stagnation point of the nose at an angle of attack of 0° is indicated for each Mach number and Reynolds number.

The effect of angle of attack on the distribution of h at a Mach number of 2.65 and a Reynolds number of 2.5×10^6 is shown in figure 10(a) for angles of attack of 0°, 10°, and 20°. At an angle of attack of 0°, the distribution of h downstream of the effects of separation is in very good agreement with the turbulent flat-plate theory of reference 11. This theory was based on the local Mach number determined from the measured static and total pressure and a boundary layer originating at the measured reattachment point on the cylinder. At an angle of attack of 10°, the turbulent flat-plate theory gives fair agreement with the

experimental data downstream of the effects of separation. However, for $x_3/y \geq 9$, the experimental values were best predicted by the turbulent, infinite-swept-cylinder theory presented in reference 12. The cylinder stagnation-line pressure was determined from equation (2). The maximum heating in the reattachment region for an angle of attack of 10° was approximately 85 percent of the stagnation value. At an angle of attack of 20°, the maximum h in the reattachment region was approximately 115 percent of the stagnation value. At an angle of attack of 20°, cross flow dominates the stagnation line in the region downstream of the effects of separation, and the resultant heat-transfer coefficients are readily predicted by turbulent swept-cylinder theory.

The effect of increasing the Mach number from 2.65 to 3.51 (fig. 10(b)) at approximately the same Reynolds number resulted in a general decrease in the heat-transfer-coefficient distribution for each angle of attack. The same good agreement between experiment and turbulent swept-cylinder theory was obtained for the portion of the cylinder downstream of the region of reattachment. The turbulent flat-plate theory of reference 11 could not be calculated for this Mach number since no pressure measurements were obtained. The magnitudes of the maximum heat-transfer coefficients in the region of reattachment expressed in terms of percent of the stagnation value on the flat front face for angles of attack of 10° and 20° are approximately 70 and 80 percent, respectively.

The distribution of h is also presented in figure 10(b) for a Mach number of 3.51, a Reynolds number of 0.8×10^6, and angles of attack of 0° and 10°. The magnitude of the distribution of h at this Reynolds number is approximately one-third of the values at the higher Reynolds number for each angle of attack. This reduced heating, similar to that measured on the conical nose at this Reynolds number, is representative of a laminar boundary layer. At an angle of attack of 10°, the experimental data are in good agreement with infinite-swept-cylinder laminar theory (ref. 9) and is approximately one-half of the turbulent swept-cylinder theory of reference 12.

A plausible explanation of the localized high heating rates occurring at an angle of attack of 20° in the reattachment region downstream of the step is that the cylinder is at a higher angle of attack relative to the velocity vector adjacent to the separation region as compared to the angle of attack relative to the free-stream velocity vector. The instability of the flow pattern in the vicinity of reattachment prevents an accurate measurement of this psuedo angle of attack.

Heat-Transfer Distribution for Five-Stage Research Vehicle Model

The heat-transfer distribution measured on the five-stage research vehicle model is presented in figure 11 for Mach numbers of 3.51 and 4.50 at nominal Reynolds numbers of 3.0×10^6 and 4.5×10^6. At stations 59 to 61 and 75 to 86, heat-transfer coefficients were measured along two diametrically opposite axial rays at meridian angles of 0° and 180° and are identified by the opened and flagged symbols, respectively. A slight difference in the level of heat-transfer coefficient occurs between thermocouples at $\phi = 0^\circ$ and 180°. The lack of pressure instrumentation prevents experimental explanation of this phenomenon. For $M = 3.51$, the heat-transfer distribution downstream of the step is of the same order of magnitude as that between stations 59 and 61 upstream of the influence of the step. Downstream of the step, the predicted values from the turbulent flat-plate theory of reference 11, based upon local Mach number and axial distance from the nose, are between the experimental data for the upper and lower meridian lines.

L 1503

Increasing the Mach number to 4.50 resulted in a general decrease in the heat-transfer distribution as shown in figure 11(b) at each Reynolds number. Fair agreement was obtained between the experimental values downstream of the step and turbulent flat-plate predictions.

CONCLUDING REMARKS

Heat-transfer coefficients on two axisymmetric models having downstream facing steps were determined in the Langley Unitary Plan wind tunnel. One model, denoted as the stepped-cylinder model, consists of a truncated conical nose with a base radius larger than the cylindrical afterbody. The second model duplicates the downstream facing step at the juncture of the fourth and fifth stages of an NASA five-stage research vehicle.

The stepped-cylinder model was tested at Mach numbers of 2.65 and 3.51, at Reynolds numbers from 0.8×10^6 to 3.1×10^6, and at angles of attack from 0° to 20°. At all angles of attack the heating rates on the conical nose in and downstream of the region of reattachment were predicted by turbulent cone theory based on the local Mach number and the local Reynolds number using a distance measured from the stagnation point on the front face. At an angle of attack of 0° the measured heat-transfer rates downstream of the region of separation were in good agreement with turbulent flat-plate theory based on local conditions and a boundary layer originating at the region of reattachment. The maximum heat-transfer coefficient in the reattachment region along the

windward meridian of the cylinder at an angle of attack of 20° was 115 percent of the measured stagnation-point value at an angle of attack of 0°. The measured heating rates downstream of the region of reattachment at angles of attack greater than 0° were in good agreement with turbulent infinite-swept-cylinder theory.

The research vehicle model was tested at Mach numbers of 3.51 and 4.50, at Reynolds numbers from 2.8×10^6 to 4.5×10^6, and at an angle of attack of 0°. The measured values downstream of the rearward facing step were in good agreement with turbulent flat-plate theory evaluated at local conditions and a local Reynolds number based on the axial length from the forward stagnation point.

The measured heating rates in the reattachment regions on both models at an angle of attack of 0° indicate no excessive heating rates above those predicted by flat-plate and conical theories.

Langley Research Center,
National Aeronautics and Space Administration,
Langley Air Force Base, Va., July 6, 1961.

REFERENCES

1. Taylor, Nancy L., Hodge, Ward F., and Burbank, Paige B.: Heat-Transfer and Pressure Measurements of a 1/7-Scale Model of a Mercury Capsule at Angles of Attack From 0° to ±20° at Mach Numbers of 3.50 and 4.44. NASA TM X-522, 1961.

2. Gadd, G. E., Cope, W. F., and Attridge, J. L.: Heat-Transfer and Skin-Friction Measurements at a Mach Number of 2.44 for a Turbulent Boundary Layer on a Flat Surface and in Regions of Separated Flow. R. & M. No. 3148, British A.R.C., 1960.

3. Naysmith, A.: Heat Transfer and Boundary Layer Measurements in a Region of Supersonic Flow Separation and Reattachment. Tech. Note No. Aero.2558, British R.A.E., May 1958.

4. Chapman, Dean R., Kuehn, Donald M., and Larson, Howard K.: Investigation of Separated Flows in Supersonic and Subsonic Streams With Emphasis on the Effect of Transition. NACA Rep. 1356, 1958. (Supersedes NACA TN 3869.)

5. Burbank, Paige B., and Hodge, B. Leon: Distribution of Heat Transfer on a 10° Cone at Angles of Attack From 0° to 15° for Mach Numbers of 2.49 to 4.65 and a Solution to the Heat-Transfer Equation That Permits Complete Machine Calculations. NASA MEMO 6-4-59L, 1959.

6. Anon.: Manual for Users of the Unitary Plan Wind Tunnel Facilities of the National Advisory Committee for Aeronautics. NACA, 1956.

7. Staff of the Computing Section, Center of Analysis (Under Direction of Zdeněk Kopal): Tables of Supersonic Flow Around Cones. Tech. Rep. No. 1 (NOrd Contract No. 9169), M.I.T., 1947.

8. Lawson, Warren A., McDearmon, R. W., and Rainey, R. W.: Investigation of the Pressure Distributions on Reentry Nose Shapes at a Mach Number of 3.55. NASA TM X-244, 1960.

9. Goodwin, Glen, Creager, Marcus O., and Winkler, Ernest L.: Investigation of Local Heat-Transfer and Pressure Drag Characteristics of a Yawed Circular Cylinder at Supersonic Speeds. NACA RM A55H31, 1956.

10. Burbank, Paige B., and Stallings, Robert L., Jr.: Heat-Transfer and Pressure Measurements on a Flat-Face Cylinder at a Mach Number Range of 2.49 to 4.44. NASA TM X-19, 1959.

11. Van Driest, E. R.: The Problem of Aerodynamic Heating. Aero. Eng. Rev., vol. 15, no. 10, Oct. 1956, pp. 26-41.

12. Beckwith, Ivan E., and Gallagher, James J.: Local Heat Transfer and Recovery Temperatures on a Yawed Cylinder at a Mach Number of 4.15 and High Reynolds Numbers. NASA TR R-104, 1961. (Supersedes NASA MEMO 2-27-59L.)

TABLE I.- RAKE PRESSURE MEASUREMENTS ON THE STEPPED-CYLINDER MODEL

[M = 2.65; $p_{t,\infty}$ = 2,882.0 lb/sq ft; T_t = 610° R]

Normal distance from surface, in.	$p_{t,2}$ for α = 0° at -			$p_{t,2}$ for α = 5° at -		$p_{t,2}$ for α = 10° at -		$p_{t,2}$ for α = 15° at -		$p_{t,2}$ for α = 20° at -	
	x_2 = 2.28 in.	x_3 = 6.50 in.	x_3 = 9.50 in.	x_3 = 6.50 in.	x_3 = 9.50 in.	x_3 = 6.50 in.	x_3 = 9.50 in.	x_3 = 6.50 in.	x_3 = 9.50 in.	x_3 = 6.50 in.	x_3 = 9.50 in.
0	1,205.9	478.7	399.0	587.9	536.2	723.5	671.7	838.3	876.4	902.0	1,033.7
.125	-------	648.8	574.0	788.1	764.2	993.2	1,075.4	1,236.7	1,283.7	1,367.4	1,415.4
.250	1,221.2	749.6	650.8	854.9	884.4	1,136.0	1,214.1	1,370.6	1,354.7	1,431.1	1,430.0
.375	-------	834.6	724.4	975.6	1,023.0	1,291.5	1,294.2	1,389.7	1,336.2	1,428.0	1,437.4
.500	-------	863.0	792.0	1,061.4	1,075.4	1,326.4	1,297.3	1,402.5	1,354.7	1,447.1	1,436.9
.750	-------	[a]141.7	[a]135.1	[a]133.5	[a]132.5	[a]158.7	[a]147.9	[a]191.2	[a]182.1	[a]226.3	[a]232.8

[a]Measurements obtained from rake static tube.

TABLE II.- PRESSURE MEASUREMENTS OBTAINED ON THE WINDWARD MERIDIAN OF THE STEPPED-CYLINDER MODEL

[M = 2.65; T_t = 610° R]

Orifice	p_l	C_p	p_l	C_p	p_l	C_p	p_l	C_p	p_l	C_p
	α = 0°; $p_{t,\infty}$ = 2,880.0 lb/sq ft		α = 5°; $p_{t,\infty}$ = 2,882.0 lb/sq ft		α = 10°; $p_{t,\infty}$ = 2,882.0 lb/sq ft		α = 15°; $p_{t,\infty}$ = 2,881.0 lb/sq ft		α = 20°; $p_{t,\infty}$ = 2,882.0 lb/sq ft	
Truncated-cone nose										
1	1,261.6	1.7176	1,275.7	1.7376	1,278.8	1.7423	1,283.7	1.7497	1,316.4	1.7980
2	1,215.6	1.6475	1,254.1	1.7047	1,269.5	1.7281	1,286.8	1.7545	1,329.1	1.8173
3	1,138.8	1.5306	1,186.3	1.6015	1,220.2	1.6531	1,265.2	1.7216	1,319.6	1.8029
4	159.6	.0396	228.0	.1435	289.7	.2374	385.7	.3834	576.9	.6737
5	214.9	.1238	369.8	.3592	483.8	.5327	592.5	.6981	749.0	.9353
6	288.5	.2359	388.3	.3874	486.9	.5374	604.8	.7168	749.0	.9353
7	294.7	.2453	388.3	.3874	486.9	.5374	604.8	.7168	745.9	.9306
8	294.7	.2453	388.3	.3874	489.9	.5420	614.1	.7309	749.0	.9353
9	297.8	.2500	397.5	.4014	493.0	.5467	623.4	.7451	745.9	.9306
10	303.9	.2593	400.6	.4061	496.1	.5514	620.3	.7404	733.1	.9112
Cylindrical afterbody										
11	43.0	-0.1380	52.2	-0.1240	76.6	-0.0868	125.5	-0.0125	230.2	0.1471
12	76.7	-.0866	122.8	-.0166	168.6	.0533	208.1	.1132	251.7	.1798
13	135.1	.0023	147.3	.0207	174.7	.0626	214.2	.1225	257.8	.1891
14	135.1	.0023	144.3	.0161	171.6	.0579	217.3	.1272	260.9	.1938
15	132.0	-.0024	141.2	.0114	171.6	.0579	214.2	.1225	267.1	.2033
16	132.0	-.0024	144.3	.0161	174.7	.0626	214.2	.1225	260.9	.1938
17	132.0	-.0024	138.1	.0067	174.7	.0626	211.2	.1179	254.8	.1845
18	132.0	-.0024	138.1	.0067	174.7	.0626	211.2	.1179	251.7	.1798
19	132.0	-.0024	138.1	.0067	171.6	.0579	208.1	.1132	251.7	.1798
20	135.1	.0023	138.1	.0067	171.6	.0579	205.1	.1086	251.7	.1798
21	135.1	.0023	138.1	.0067	168.6	.0533	202.0	.1039	251.7	.1798

TABLE III.- LOCAL HEAT-TRANSFER MEASUREMENTS OBTAINED

ON THE STEPPED-CYLINDER MODEL

(a) M = 2.65

Thermo-couple	$T_{w,e}/T_t$	T_w, deg	h	N_{St}	$T_{w,e}/T_t$	T_w, deg	h	N_{St}	$T_{w,e}/T_t$	T_w, deg	h	N_{St}	$T_{w,e}/T_t$	T_w, deg	h	N_{St}	$T_{w,e}/T_t$	T_w, deg	h	N_{St}
	$\alpha = 0^o$; $T_t = 710^o$ R; $p_{t,\infty} = 2{,}881.5$ lb/sq ft				$\alpha = 5^o$; $T_t = 712^o$ R; $p_{t,\infty} = 2{,}884.6$ lb/sq ft				$\alpha = 10^o$; $T_t = 711^o$ R; $p_{t,\infty} = 2{,}939.3$ lb/sq ft				$\alpha = 15^o$; $T_t = 713^o$ R; $p_{t,\infty} = 2{,}885.3$ lb/sq ft				$\alpha = 20^o$; $T_t = 709^o$ R; $p_{t,\infty} = 2{,}831.8$ lb/sq ft			
1	1.00000	646.5	0.01298	0.002842	0.99885	647.5	0.01400	0.003059	0.99603	652.9	0.01514	0.003245	0.99771	641.9	0.01510	0.003300	0.99829	652.2	0.01512	0.003371
2	.99545	645.9	.01341	.002936	.99599	649.9	.01462	.003194	.99433	657.2	.01641	.003517	.99600	648.5	.01746	.003816	.99829	661.5	.01808	.004030
3	.98862	642.9	.01307	.002862	.99142	648.9	.01462	.003194	.98980	658.5	.01743	.003735	.99315	652.2	.01939	.004238	.99545	667.2	.02165	.004826
4	.98009	636.2	.01122	.002457	.98399	644.9	.01370	.002993	.98414	657.2	.01691	.003624	.98744	652.5	.01902	.004157	.99148	669.2	.02165	.004826
5	.96759	606.9	.00677	.001482	.97599	628.5	.01017	.002222	.97564	648.5	.01392	.002983	.97831	646.2	.01618	.003536	.98239	670.5	.01964	.004378
6	.97157	625.5	.00903	.001977	.97713	657.9	.01547	.003380	.97168	671.5	.02156	.004620	.98117	682.2	.02836	.006198	.98693	682.5	.02682	.005979
7	.96531	634.5	.01313	.002875	.96856	644.5	.01572	.003434	.97055	664.5	.01837	.003937	.97946	655.9	.02144	.004686	.98523	670.5	.02191	.004884
8	.96815	628.5	.01147	.002512	.97028	637.9	.01352	.002954	.97055	664.8	.01675	.003590	.97774	650.2	.01982	.004332	.98239	665.2	.02188	.004878
9	.97441	631.2	.01079	.002363	.97599	640.5	.01385	.003026	.97621	653.5	.01692	.003626	.98231	651.5	.01978	.004323	.98580	678.2	.01858	.004142
10	.97327	628.5	.01118	.002448	.97485	637.9	.01365	.002982	.97451	650.9	.01619	.003470	.98060	648.2	.01852	.004048	.98466	663.2	.02016	.004494
11	.97327	629.9	.01064	.002330	.97313	638.2	.01402	.003063	.97281	650.9	.01718	.003682	.97774	647.5	.02017	.004408	.98012	661.9	.02130	.004748
13	.99943	602.9	.00291	.000637	.98971	604.5	.00438	.000957	.98017	614.5	.00662	.001419	.96805	610.5	.00997	.002179	.94490	623.9	.01120	.002497
14	.97327	602.2	.00588	.001288	.95085	600.5	.00829	.001811	.93487	605.2	.01083	.002321	.92583	595.2	.01322	.002889	.92105	606.5	.01508	.003362
15	.94484	591.5	.00694	.001520	.92570	587.2	.00896	.001958	.91958	593.5	.01064	.002280	.92069	587.5	.01191	.002603	.92843	606.5	.01364	.003041
16	.93461	585.5	.00678	.001485	.92627	584.9	.00804	.001757	.92354	592.9	.00939	.002012	.92697	590.5	.01093	.002389	.93866	609.5	.01195	.002664
17	.93120	581.9	.00680	.001489	.92570	582.5	.00778	.001700	.92524	591.9	.00927	.001987	.92982	590.5	.01095	.002393	.94263	609.5	.01173	.002615
19	.93518	581.5	.00627	.001373	.93084	582.9	.00718	.001569	.93034	592.5	.00853	.001828	.93381	590.5	.01001	.002188	.94718	609.5	.01078	.002403
20	.93916	583.2	.00592	.001296	.93770	585.9	.00688	.001503	.93770	595.9	.00816	.001749	.94237	594.2	.00959	.002096	.95513	613.2	.01022	.002278
21	.93574	581.2	.00608	.001331	.93313	583.2	.00695	.001518	.93204	592.9	.00844	.001809	.93552	590.5	.00998	.002181	.94945	610.5	.01061	.002365
22	.93518	580.5	.00598	.001309	.93256	581.9	.00696	.001521	.93204	591.9	.00825	.001768	.93438	589.2	.00974	.002129	.94831	609.2	.01053	.002347
23	.93688	580.9	.00596	.001305	.93541	582.9	.00678	.001481	.93487	592.9	.00822	.001762	.93667	589.9	.00973	.002127	.95058	609.9	.01045	.002330
24	.93574	580.5	.00584	.001279	.93484	582.5	.00660	.001442	.93317	591.9	.00817	.001751	.93552	589.5	.00952	.002081	.94774	609.2	.01050	.002341
25	.93688	580.5	.00582	.001274	.93541	582.9	.00671	.001466	.93430	592.5	.00803	.001721	.93667	590.5	.00962	.002103	.94831	610.2	.01063	.002370
26	.93972	582.5	.00575	.001259	.93770	584.5	.00668	.001459	.93770	594.5	.00786	.001684	.93952	592.5	.00969	.002118	.95172	612.5	.01048	.002336
28	.93972	581.2	.00558	.001222	.93770	583.5	.00652	.001424	.93600	592.9	.00770	.001650	.93838	590.5	.00944	.002063	.94945	611.5	.01056	.002354
30	.94257	583.5	.00557	.001220	.94170	586.2	.00646	.001411	.93940	595.2	.00781	.001674	.94294	594.2	.00945	.002065	.95342	614.9	.01062	.002367
31	.94257	582.9	.00553	.001211	.94056	585.9	.00638	.001394	.93770	594.5	.00773	.001657	.94180	593.9	.00956	.002089	.95115	614.2	.01099	.002450
32	.94370	583.2	.00557	.001220	.94170	586.2	.00663	.001448	.93883	594.9	.00799	.001712	.94351	594.5	.00978	.002138	.95286	614.9	.01130	.002519
33	.94086	581.9	.00545	.001193	.93884	584.2	.00631	.001379	.93373	591.9	.00780	.001672	.93895	591.9	.00943	.002061	.94661	610.9	.01073	.002392
34	.94200	582.9	.00562	.001231	.93999	585.2	.00653	.001427	.93600	594.2	.00820	.001757	.94180	594.5	.00991	.002166	.95058	614.5	.01156	.002577
35	.94143	582.5	.00551	.001206	.93884	584.5	.00649	.001418	.93430	593.2	.00812	.001740	.94009	593.5	.00989	.002162	.94831	613.5	.01152	.002568
36	.94086	582.9	.00563	.001233	.93770	584.2	.00661	.001444	.93317	592.9	.00838	.001796	.93895	593.5	.01020	.002229	.94831	614.9	.01197	.002668
37	.94598	584.9	.00543	.001189	.94342	587.2	.00631	.001379	.93996	596.2	.00788	.001689	.94522	597.2	.00975	.002131	.95286	617.2	.01151	.002566
38	.94769	585.2	.00534	.001169	.94399	587.2	.00632	.001381	.93996	596.5	.00793	.001699	.94579	597.9	.00998	.002181	.95286	617.2	.01162	.002590
39	.94314	582.9	.00523	.001145	.93999	584.5	.00619	.001352	.93543	593.9	.00801	.001717	.94066	594.9	.01011	.002210	.94661	614.5	.01197	.002668
40	.94712	584.5	.00519	.001136	.94284	585.9	.00619	.001352	.93883	595.5	.00787	.001687	.94351	595.9	.00984	.002151	.94945	614.9	.01139	.002539
46	.93745	581.9	.00582	.001274	.93313	582.5	.00681	.001488	.93430	591.9	.00774	.001659	.93781	588.2	.00890	.001945	.94888	607.2	.00975	.002173
47	.94029	581.9	.00552	.001209	.93770	583.5	.00650	.001420	.93600	592.5	.00758	.001624	.93895	589.2	.00886	.001936	.94718	607.2	.01005	.002240
48	.94029	581.5	.00547	.001198	.93713	583.2	.00628	.001372	.93657	591.9	.00755	.001618	.93895	589.2	.00895	.001956	.94661	606.9	.01015	.002263
50	.93745	580.5	.00569	.001246	.93599	581.5	.00629	.001374	.93260	587.2	.00710	.001522	.93438	582.2	.00796	.001740	.94150	598.5	.00879	.001959
52	.93631	580.9	.00575	.001259	.84740	607.5	.03871	.008457	.92920	582.2	.00631	.001352	.92640	572.9	.00659	.001440	.93639	586.2	.00666	.001485
53	.94029	582.2	.00541	.001185	.93770	581.9	.00596	.001302	.93260	583.9	.00607	.001301	.93267	576.2	.00651	.001423	.93923	588.9	.00671	.001496
55	.93745	580.9	.00572	.001252	.91084	577.2	.00697	.001523	.92524	571.2	.00465	.000997	.91898	555.5	.00382	.000835	.92900	564.9	.00351	.000782
56	.94086	582.2	.00549	.001202	.93770	578.9	.00556	.001215	.92864	571.2	.00425	.000911	.92411	557.5	.00365	.000798	.93355	567.2	.00347	.000774
58	.94200	583.2	.00561	.001228	.93941	579.2	.00545	.001191	.93657	571.2	.00355	.000761	.92868	556.2	.00274	.000599	.95002	575.9	.00305	.000680
59	.93745	580.9	.00574	.001257	.94227	580.2	.00533	.001164	.93770	578.5	.00473	.001014	.92126	552.9	.00330	.000721	.93525	565.2	.00297	.000662
60	.94200	579.9	.00484	.001060	.95256	581.9	.00425	.000929	.95865	586.2	.00371	.000795	.95549	584.5	.00508	.001110	.94150	582.5	.00476	.001061

[redacted]

TABLE III.- LOCAL HEAT-TRANSFER MEASURMENTS OBTAINED

ON THE STEPPED-CYLINDER MODEL - Continued

(b) M = 3.51

Thermo-couple	$T_{w,e}/T_t$	T_w, deg	h	N_{St}	$T_{w,e}/T_t$	T_w, deg	h	N_{St}
	$\alpha = 0^o$; $T_t = 715^oR$; $p_{t,\infty} = 1,445.1$ lb/sq ft				$\alpha = 10^o$; $T_t = 708^o$ R; $p_{t,\infty} = 1,440.7$ lb/sq ft			
1	1.00619	642.5	0.00631	0.006149	0.99430	629.5	0.00725	0.007069
2	.99887	641.2	.00651	.006344	.99202	633.2	.00781	.007615
3	.98817	635.9	.00644	.006276	.98519	632.2	.00781	.007615
4	.97860	629.2	.00582	.005672	.97835	628.5	.00717	.006991
5	.96452	606.5	.00359	.003499	.96753	610.9	.00491	.004787
6	.96339	597.2	.00281	.002738	.97038	609.9	.00464	.004524
7	.95889	590.5	.00248	.002417	.96696	599.9	.00384	.003744
8	.95720	586.2	.00222	.002163	.96696	594.5	.00346	.003374
9	.96564	588.2	.00182	.001774	.97380	595.9	.00302	.002945
10	.96959	588.9	.00176	.001715	.97493	595.5	.00276	.002691
11	.97353	589.9	.00163	.001588	.97152	594.5	.00294	.002867
13	-------	-----	-------	--------	1.00854	593.9	.00062	.000605
14	-------	-----	-------	--------	.99088	595.5	.00181	.001765
15	1.01464	597.9	.00011	.000107	.97721	592.5	.00228	.002223
16	1.00225	591.9	.00021	.000205	.97038	585.9	.00210	.002048
17	.99380	589.2	.00045	.000439	.96354	579.2	.00178	.001736
19	.99267	590.2	.00062	.000604	.96240	576.5	.00164	.001599
20	.99662	593.2	.00068	.000663	.96924	582.5	.00142	.001385
21	.99042	590.2	.00075	.000731	.96013	579.2	.00156	.001521
22	.98986	589.9	.00070	.000682	.95842	573.5	.00154	.001502
23	.99042	590.5	.00079	.000770	.95899	574.5	.00166	.001619
24	.98873	589.5	.00071	.000692	.95671	573.2	.00155	.001511
25	.98873	589.9	.00081	.000789	.95614	573.2	.00156	.001521
26	.99098	590.5	.00075	.000731	.95785	574.5	.00160	.001560
28	.98986	590.2	.00079	.000770	.95614	573.5	.00171	.001667
30	.99098	590.2	.00069	.000672	.95728	574.9	.00171	.001667
31	.98930	589.2	.00075	.000731	.95500	573.5	.00166	.001619
32	.98930	590.5	.00080	.000780	.95500	573.5	.00177	.001726
33	.98592	587.2	.00080	.000780	.95101	570.9	.00162	.001580
34	.98817	589.2	.00073	.000711	.95329	572.5	.00176	.001716
35	.98648	588.5	.00085	.000828	.95215	571.5	.00171	.001667
36	.98479	588.2	.00094	.000916	.95158	570.9	.00169	.001648
37	.98761	590.2	.00093	.000906	.95443	572.9	.00169	.001648
38	.98986	591.9	.00096	.000936	.95614	573.9	.00168	.001638
39	.98761	590.9	.00102	.000994	.95500	573.2	.00163	.001589
40	.99774	597.2	.00099	.000965	.96468	578.5	.00167	.001628
46	.99155	592.2	.00080	.000780	.95728	571.2	.00135	.001316
47	.99098	591.2	.00080	.000780	.95500	571.2	.00143	.001394
48	.98986	589.9	.00081	.000789	.95272	570.2	.00153	.001492
50	.99042	589.5	.00073	.000711	.95272	567.5	.00120	.001170
52	.99211	591.2	.00075	.000731	.95614	567.9	.00106	.001034
53	.99267	590.9	.00065	.000633	.95557	567.9	.00105	.001024
55	.99042	590.9	.00079	.000770	.95500	564.5	.00070	.000683
56	.99155	591.2	.00078	.000760	.95557	563.5	.00074	.000722
58	.98986	588.9	.00085	.000828	.96354	564.2	.00022	.000215
59	.98817	589.9	.00083	.000809	.97266	572.9	.00059	.000575
60	.99098	588.5	.00062	.000604	.98462	581.5	.00076	.000741

[redacted]

TABLE III.- LOCAL HEAT-TRANSFER MEASUREMENTS OBTAINED

ON THE STEPPED-CYLINDER MODEL - Concluded

(b) M = 3.51 - Concluded

Thermocouple	$T_{w,e}/T_t$	T_w, deg	h	N_{St}	$T_{w,e}/T_t$	T_w, deg	h	N_{St}	$T_{w,e}/T_t$	T_w, deg	h	N_{St}	$T_{w,e}/T_t$	T_w, deg	h	N_{St}	$T_{w,e}/T_t$	T_w, deg	h	N_{St}
	$\alpha = 0^\circ$; $T_t = 714^\circ$ R; $p_{t,\infty} = 5{,}059.0$ lb/sq ft				$\alpha = 5^\circ$; $T_t = 717^\circ$ R; $p_{t,\infty} = 5{,}053.0$ lb/sq ft				$\alpha = 10^\circ$; $T_t = 716^\circ$ R; $p_{t,\infty} = 5{,}049.0$ lb/sq ft				$\alpha = 15^\circ$; $T_t = 717^\circ$ R; $p_{t,\infty} = 5{,}024.0$ lb/sq ft				$\alpha = 20^\circ$; $T_t = 718^\circ$ R; $p_{t,\infty} = 5{,}066.0$ lb/sq ft			
1	1.00172	648.5	0.01203	0.003349	1.00000	647.9	0.01273	0.003554	0.99484	644.5	0.01324	0.003697	0.99487	646.9	0.01346	0.003785	0.99715	650.5	0.01327	0.003691
2	.99713	647.5	.01212	.003374	.99656	650.2	.01364	.003809	.99312	649.5	.01462	.004082	.99374	653.5	.01541	.004334	.99772	659.9	.01559	.004337
3	.98852	643.6	.01194	.003324	.99026	648.2	.01415	.003951	.98796	650.5	.01518	.004239	.98975	656.5	.01636	.004601	.99488	664.8	.01653	.004598
4	.97934	635.9	.01068	.002973	.98166	651.2	.01212	.003384	.98051	647.2	.01491	.004163	.98350	664.5	.01606	.004517	.99033	680.8	.01689	.004698
5	.96327	601.9	.00553	.001539	.96849	615.9	.00760	.002122	.96847	626.5	.00981	.002739	.97383	641.9	.01194	.003358	.98237	680.8	.01321	.003675
6	.96557	605.2	.00544	.001514	.97651	633.9	.00928	.002591	.97535	651.9	.01364	.003809	.97838	665.5	.01731	.004868	.98578	677.5	.02094	.005825
7	.96614	611.2	.00587	.001634	.97135	634.2	.01103	.003080	.97134	643.9	.01454	.004060	.97610	655.5	.01716	.004826	.98351	665.8	.01802	.005013
8	.96844	614.9	.00734	.002043	.97135	629.9	.01117	.003119	.97134	638.5	.01397	.003901	.97553	660.5	.01620	.004556	.98180	660.9	.01787	.004971
9	.97532	628.5	.00762	.002121	.97708	632.9	.01089	.003041	.97535	641.2	.01378	.003848	.97724	649.5	.01585	.004458	.98237	678.8	.01556	.004328
10	.97417	620.5	.00764	.002127	.97479	630.2	.01008	.002815	.97306	638.9	.01378	.003848	.97383	658.5	.01611	.004531	.97782	658.2	.01802	.005013
11	.97360	621.5	.00856	.002383	.97250	639.5	.01085	.003030	.97019	648.5	.01400	.003909	.96472	611.9	.00829	.002331	.93859	619.5	.00929	.002584
13	1.04992	618.5	.00131	.000365	1.02291	615.9	.00308	.000860	.98739	617.9	.00569	.001589	.91125	580.2	.00906	.002548	.94143	603.2	.00956	.002659
14	1.00975	611.5	.00350	.000974	.95532	596.5	.00694	.001938	.92090	582.5	.00825	.002304	.91011	574.9	.00773	.002174	.95167	603.2	.00781	.002173
15	.95409	587.5	.00490	.001364	.91923	573.2	.00623	.001740	.90772	566.9	.00673	.001879	.92092	580.9	.00725	.002039	.95678	603.5	.00673	.001872
16	.93171	574.5	.00475	.001322	.91808	568.2	.00519	.001449	.91288	566.9	.00579	.001617	.92661	583.5	.00729	.002050	.95280	602.5	.00714	.001986
17	.92483	567.9	.00449	.001250	.91751	564.9	.00496	.001385	.91574	566.5	.00552	.001541	.93457	585.9	.00678	.001907	.95110	602.2	.00732	.002036
19	.92770	566.5	.00406	.001130	.92266	565.5	.00438	.001223	.92205	568.5	.00523	.001460	.94310	589.9	.00640	.001800	.95621	605.5	.00729	.002028
20	.93630	570.2	.00379	.001055	.93068	569.2	.00409	.001142	.93294	573.9	.00493	.001377	.94310	589.9	.00651	.001831	.94712	602.5	.00809	.002250
21	.92942	566.2	.00390	.001086	.92496	565.9	.00428	.001195	.92606	570.2	.00512	.001430	.93741	586.2	.00642	.001806	.94370	601.2	.00823	.002289
22	.92884	565.2	.00358	.000997	.92553	565.5	.00421	.001176	.92549	569.9	.00500	.001396	.93628	585.2	.00626	.001761	.94370	601.9	.00858	.002387
23	.93171	565.5	.00353	.000983	.92839	566.5	.00414	.001156	.92835	570.9	.00504	.001407	.93798	585.9	.00627	.001763	.94029	601.2	.00868	.002415
24	.93056	564.9	.00347	.000966	.92782	565.9	.00401	.001120	.92835	570.5	.00494	.001379	.93685	585.5	.00625	.001758	.93972	601.5	.00892	.002481
25	.93171	565.2	.00343	.000955	.92782	565.9	.00397	.001108	.92950	571.5	.00490	.001368	.93741	586.2	.00633	.001780	.94086	602.9	.00885	.002462
26	.93515	567.2	.00338	.000941	.93183	567.9	.00392	.001095	.93236	573.9	.00492	.001374	.93969	587.5	.00631	.001775	.93745	599.9	.00877	.002440
28	.93515	566.2	.00318	.000885	.93183	566.9	.00374	.001044	.93236	572.5	.00489	.001365	.93628	585.5	.00653	.001836	.94029	601.9	.00865	.002406
30	.93917	568.5	.00309	.000860	.93584	569.5	.00375	.001047	.93695	575.9	.00479	.001337	.93741	587.5	.00657	.001848	.93859	600.9	.00861	.002395
31	.93802	567.9	.00313	.000871	.93412	568.9	.00371	.001036	.93580	575.9	.00486	.001357	.93514	586.9	.00700	.001969	.93916	600.5	.00883	.002456
32	.93917	568.5	.00325	.000905	.93584	569.9	.00383	.001069	.93638	575.9	.00493	.001377	.93457	586.9	.00681	.001915	.93461	597.5	.00837	.002328
33	.93573	565.9	.00304	.000846	.93011	566.2	.00365	.001019	.93179	572.9	.00483	.001349	.93002	584.2	.00721	.002028	.93859	600.2	.00868	.002415
34	.94032	568.5	.00313	.000871	.93469	568.9	.00380	.001061	.93580	575.5	.00505	.001410	.93229	586.9	.00723	.002033	.93688	598.9	.00844	.002348
35	.93975	567.9	.00308	.000857	.93355	568.2	.00377	.001053	.93351	575.2	.00501	.001399	.92945	585.9	.00743	.002090	.93631	599.2	.00874	.002431
36	.93860	567.9	.00317	.000882	.93298	567.9	.00376	.001050	.93179	574.2	.00517	.001444	.92717	584.9	.00738	.002075	.93972	601.2	.00855	.002378
37	.94491	571.2	.00297	.000827	.93870	571.2	.00367	.001025	.93752	577.5	.00506	.001413	.93116	587.5	.00729	.002050	.94029	601.9	.00857	.002384
38	.94835	572.2	.00294	.000818	.94099	572.2	.00369	.001030	.93752	577.9	.00498	.001391	.93173	587.9	.00739	.002078	.93631	599.5	.00863	.002401
39	.94376	569.5	.00296	.000824	.93756	569.9	.00370	.001033	.93179	575.2	.00522	.001458	.92661	584.9	.00713	.002005	.93802	600.5	.00855	.002378
40	.95122	573.2	.00278	.000774	.94386	573.2	.00354	.000988	.93580	577.2	.00513	.001432	.92945	585.9	.00574	.001614	.94029	597.5	.00787	.002189
46	.93343	566.9	.00353	.000983	.92954	566.5	.00395	.001103	.92950	569.9	.00461	.001287	.94026	584.5	.00584	.001642	.93518	595.2	.00794	.002209
47	.93630	566.9	.00325	.000905	.93183	567.2	.00371	.001036	.93294	571.5	.00453	.001265	.93571	582.9	.00619	.001741	.93120	592.9	.00793	.002206
48	.93745	567.2	.00315	.000877	.93355	567.2	.00355	.000991	.93351	571.9	.00461	.001287	.93116	581.2	.00493	.001386	.92949	586.2	.00690	.001919
50	.93458	565.9	.00331	.000921	.93126	565.5	.00363	.001014	.92778	565.9	.00406	.001134	.93173	575.9	.00387	.001088	.93006	576.9	.00495	.001377
52	.93343	566.5	.00342	.000952	.92897	564.5	.00361	.001008	.92434	561.2	.00365	.001019	.92661	567.2	.00387	.001088	.92665	577.2	.00538	.001497
53	.93860	568.2	.00306	.000852	.93469	566.9	.00337	.000941	.92835	562.9	.00353	.000986	.92945	568.9	.00210	.000591	.91698	554.5	.00264	.000734
55	.93688	567.2	.00326	.000907	.93240	563.9	.00317	.000885	.92090	551.5	.00252	.000704	.91466	548.9	.00213	.000599	.91698	554.2	.00260	.000723
56	.94089	568.5	.00314	.000874	.93756	565.2	.00298	.000832	.92319	551.9	.00227	.000634	.91693	549.9	.00107	.000301	.93518	557.2	.00114	.000317
58	.94204	569.5	.00308	.000857	.94500	571.5	.00277	.000773	.93064	551.2	.00122	.000341	.92149	545.9	.00161	.000453	.93518	558.2	.00165	.000459
59	.93802	568.2	.00323	.000899	.93756	566.2	.00316	.000882	.92778	557.9	.00275	.000768	.91181	543.2	.00285	.000802	.93233	566.5	.00255	.000709
60	.94778	569.5	.00259	.000721	.94672	568.9	.00257	.000718	.94727	566.5	.00229	.000639	.93400	564.9						

TABLE IV.- LOCAL HEAT-TRANSFER MEASUREMENTS OBTAINED ON THE FIVE-STAGE RESEARCH VEHICLE MODEL

$[\alpha = 0^\circ]$

Thermocouple	$T_{w,e}/T_t$	T_w, deg	h	N_{St}	$T_{w,e}/T_t$	T_w, deg	h	N_{St}	$T_{w,e}/T_t$	T_w, deg	h	N_{St}	$T_{w,e}/T_t$	T_w, deg	h	N_{St}
	M = 3.51								M = 4.50							
	T_t = 714° R; $p_{t,\infty}$ = 5,088.0 lb/sq ft				T_t = 711° R; $p_{t,\infty}$ = 8,066.0 lb/sq ft				T_t = 671° R; $p_{t,\infty}$ = 8,637.0 lb/sq ft				T_t = 676° R; $p_{t,\infty}$ = 12,261.0 lb/sq ft			
1	0.94008	581.5	0.00273	0.000750	0.94023	580.5	0.00364	0.000632	0.94312	567.9	0.00147	0.000550	0.93909	570.5	0.00177	0.000468
2	.93952	580.9	.00270	.000742	.94023	579.9	.00354	.000614	.94312	567.5	.00136	.000509	.93909	570.5	.00169	.000477
3	.94008	580.5	.00258	.000709	.93967	578.9	.00345	.000599	.94255	567.5	.00147	.000550	.93853	570.2	.00169	.000447
4	.93815	580.2	.00237	.000656	.93991	578.5	.00305	.000530	.93892	568.2	.00149	.000560	.93499	571.5	.00192	.000508
5	.93703	579.2	.00229	.000634	.93822	577.9	.00312	.000542	.93724	567.2	.00148	.000557	.93332	570.5	.00184	.000487
6	.93536	578.2	.00230	.000637	.93766	577.5	.00312	.000542	.93668	567.2	.00139	.000523	.93276	570.2	.00194	.000514
7	.94568	588.5	.00413	.001135	.94474	587.5	.00559	.000970	.94368	569.9	.00242	.000906	.94077	573.9	.00279	.000738
8	.94960	590.5	.00395	.001086	.94756	589.2	.00577	.001001	.94424	569.9	.00211	.000790	.94021	573.5	.00273	.000722
9	.94848	590.2	.00414	.001138	.94644	589.2	.00567	.000984	.94255	568.9	.00215	.000805	.94077	575.2	.00264	.000699
10	.94456	587.9	.00412	.001133	.94362	587.5	.00577	.001001	.94255	569.2	.00207	.000775	.94077	575.2	.00264	.000699
11	.94792	590.2	.00417	.001146	.94587	588.9	.00567	.000984	.94481	572.2	.00205	.000768	.94356	575.2	.00260	.000688
12	.96472	574.9	.00028	.000077	.94926	562.9	.00047	.000082	-------	-----	-------	--------	-------	-----	-------	--------
13	.96248	573.9	.00032	.000088	.94869	562.5	.00052	.000090	.98085	579.9	.00017	.000064	-------	-----	-------	--------
14	.96136	573.9	.00054	.000148	.94813	562.9	.00074	.000128	.97747	578.5	.00026	.000097	.96871	578.2	.00036	.000095
15	.95408	572.9	.00101	.000278	.94193	566.5	.00129	.000224	.97071	576.5	.00059	.000221	.96200	576.2	.00073	.000193
16	.93952	576.2	.00231	.000635	.93121	568.9	.00302	.000524	.95720	574.5	.00127	.000476	.94580	572.9	.00176	.000466
17	.93112	573.5	.00274	.000753	.92501	567.9	.00354	.000614	.94762	569.9	.00158	.000592	.93518	567.5	.00205	.000542
18	.92496	570.5	.00292	.000803	.91994	565.9	.00431	.000748	.93861	566.2	.00169	.000633	.92624	570.2	.00188	.000497
19	.92272	569.5	.00308	.000847	.91881	565.5	.00401	.000696	.93185	560.9	.00170	.000637	.92065	559.5	.00220	.000582
20	.91992	567.9	.00312	.000858	.91768	565.2	.00409	.000710	.92735	558.2	.00175	.000655	.91786	557.5	.00219	.000579
21	.91824	566.5	.00314	.000863	.91768	564.9	.00411	.000713	.92341	555.9	.00172	.000644	.91507	555.9	.00208	.000550
22	.91936	566.9	.00300	.000825	.91881	564.9	.00401	.000696	.92116	555.5	.00176	.000659	.91451	554.9	.00202	.000535
23	.92048	567.2	.00305	.000838	.91994	565.9	.00398	.000691	.92228	554.5	.00161	.000603	.91618	555.5	.00200	.000529
24	.91992	566.9	.00298	.000819	.91994	565.9	.00395	.000685	.92116	553.5	.00160	.000599	.91563	555.2	.00194	.000513
25	.92160	567.9	.00301	.000827	.92163	566.9	.00403	.000699	.92172	555.2	.00149	.000558	.91674	555.9	.00195	.000516
26	.92272	568.5	.00294	.000808	.92219	567.5	.00403	.000699	.92228	554.2	.00154	.000577	.91786	556.2	.00176	.000466
27	.92496	569.5	.00314	.000863	.92445	568.9	.00404	.000701	.92397	557.2	.00139	.000520	.92289	558.9	.00167	.000442
28	.92608	570.2	.00298	.000819	.92558	569.9	.00409	.000710	.92510	557.9	.00139	.000520	.92121	557.9	.00181	.000479
29	.92552	569.9	.00296	.000814	.92501	569.5	.00407	.000706	.92510	555.2	.00144	.000539	.92121	557.9	.00170	.000450
30	.92776	571.2	.00287	.000789	.92840	571.2	.00406	.000704	.92735	558.9	.00138	.000517	.92401	559.2	.00179	.000474
31	.92776	571.2	.00288	.000792	.92727	570.5	.00401	.000696	.92735	556.2	.00143	.000535	.92401	559.2	.00177	.000468
32	.92944	572.2	.00304	.000836	.92840	571.9	.00423	.000734	.92904	557.2	.00145	.000543	.92568	560.2	.00175	.000463
33	.92944	571.9	.00295	.000811	.92783	571.2	.00422	.000732	.93017	557.9	.00144	.000539	.92568	560.5	.00171	.000452
34	.93056	572.9	.00294	.000808	.92896	572.2	.00413	.000717	.93073	558.5	.00133	.000498	.92736	561.5	.00169	.000447
35	.94762	568.5	.00040	.000111	.93261	556.9	.00079	.000137	-------	-----	-------	--------	.96555	578.2	.00023	.000061
36	.94929	569.9	.00050	.000138	.93373	557.9	.00082	.000143	.97422	578.9	.00021	.000079	.96666	579.2	.00026	.000069
37	.94873	570.9	.00076	.000210	.93373	559.9	.00118	.000205	.97198	578.9	.00035	.000132	.96555	579.5	.00043	.000114
38	.94818	573.9	.00122	.000338	.93373	563.9	.00198	.000344	.97030	579.9	.00066	.000248	.96388	580.9	.00082	.000217
39	.94149	579.5	.00239	.000662	.93092	572.5	.00348	.000605	.96358	581.2	.00144	.000542	.95388	581.2	.00196	.000519
40	.92868	574.2	.00283	.000784	.92250	568.9	.00387	.000673	.95125	575.5	.00182	.000685	.93776	572.9	.00225	.000596
41	.92255	570.2	.00289	.000800	.91913	566.2	.00385	.000669	.94116	569.9	.00179	.000673	.92776	566.9	.00246	.000651
42	.91865	567.9	.00283	.000784	.91745	564.9	.00383	.000666	.93164	563.9	.00180	.000677	.91832	561.5	.00247	.000654
43	.91865	566.2	.00271	.000750	.91801	563.2	.00351	.000610	.92604	560.5	.00181	.000681	.91498	559.2	.00230	.000609
45	.91642	564.9	.00260	.000720	.91745	563.2	.00351	.000610	.91987	556.2	.00168	.000632	.91165	556.5	.00216	.000572
46	.91698	565.2	.00259	.000717	.91857	563.9	.00342	.000595	.91931	555.5	.00160	.000602	.91276	556.5	.00211	.000559
47	.91976	566.5	.00243	.000673	.92081	564.5	.00333	.000579	.91987	555.5	.00159	.000598	.91443	557.5	.00208	.000551
48	.92088	567.2	.00242	.000670	.92306	565.9	.00326	.000567	.91987	555.9	.00159	.000598	.91498	559.5	.00199	.000527
49	.92143	567.2	.00244	.000676	.92306	565.9	.00330	.000574	.92099	556.2	.00155	.000583	.91665	561.5	.00190	.000503
50	.92199	567.5	.00242	.000670	.92306	565.5	.00329	.000572	.92155	556.5	.00154	.000579	.91776	559.2	.00202	.000535
51	.92199	567.2	.00235	.000651	.92306	565.2	.00322	.000560	.92155	556.2	.00148	.000557	.91776	559.2	.00195	.000516
52	.92478	568.5	.00237	.000656	.92531	566.2	.00311	.000541	.92323	559.5	.00139	.000523	.91998	560.2	.00193	.000511
53	.92756	570.2	.00232	.000642	.92812	568.2	.00317	.000551	.92547	560.9	.00138	.000519	.92221	561.9	.00184	.000487
54	.92533	568.9	.00233	.000645	.92643	567.2	.00313	.000544	.92491	558.2	.00149	.000560	.92165	561.2	.00193	.000511
55	.92422	568.5	.00235	.000651	.92531	567.5	.00325	.000565	.92604	560.9	.00137	.000515	.92276	561.9	.00181	.000479
56	.92700	570.2	.00232	.000642	.92812	568.5	.00326	.000567	.92772	561.9	.00137	.000515	.92443	562.9	.00192	.000508
57	.92923	571.5	.00234	.000648	.92980	569.9	.00327	.000568	.92940	560.5	.00145	.000545	.92665	564.5	.00195	.000516

Orifice	Thermocouple	Skin thickness, b, in.	Meridian angle, ϕ, deg	$\frac{x_1}{r}$	$\frac{x_2}{r}$	$\frac{x_3}{y}$
-	1	0.0325	0	0.00		
I	2	.0322	0	.50		
2	3	.0325	0	.72		
3	4	.0306	0	.86		
4	5	.0230	0		0.15	
5	6	.0250	0		.61	
6	7	.0264	0		1.22	
7	8	.0285	0		1.82	
8	9	.0285	0		2.43	
9	10	.0283	0		3.04	
10	11	.0290	0		3.59	
-	12	.0310	0			0.83
11	13	.0315	0			1.67
12	14	.0315	0			2.50
-	15	.0305	0			3.33
13	16	.0295	0			4.17
-	17	.0305	0			5.00
-	18	.0305	0			5.42
14	19	.0305	0			5.83
-	20	.0305	0			6.25
-	21	.0310	0			6.67
-	22	.0310	0			7.08
15	23	.0315	0			7.50
-	24	.0310	0			7.92
-	25	.0310	0			8.33
-	26	.0310	0			8.75
16	27	.0310	0			9.17
-	28	.0305	0			9.58
-	29	.0305	0			10.00
-	30	.0305	0			10.42
17	31	.0305	0			10.83
-	32	.0315	0			11.25
-	33	.0305	0			11.67
18	34	.0310	0			12.50
-	35	.0305	0			13.33
19	36	.0305	0			14.17
-	37	.0305	0			15.00
20	38	.0305	0			15.83
-	39	.0305	0			16.67
21	40	.0305	0			17.50
-	41	.0300	0			18.33
-	42	.0300	0			19.17
-	43	.0310	15			8.33
-	44	.0310	15			10.00
-	45	.0310	15			11.67
-	46	.0310	30			8.33
-	47	.0305	30			10.00
-	48	.0310	30			11.67
-	49	.0310	45			8.33
-	50	.0310	45			10.00
-	51	.0315	45			11.67
-	52	.0305	60			8.33
-	53	.0305	60			10.00
-	54	.0315	60			11.67
-	55	.0305	90			10.00
-	56	.0310	90			11.67
-	57	.0295	120			8.33
-	58	.0310	120			11.67
-	59	.0310	150			10.00
-	60	.0315	180			10.00

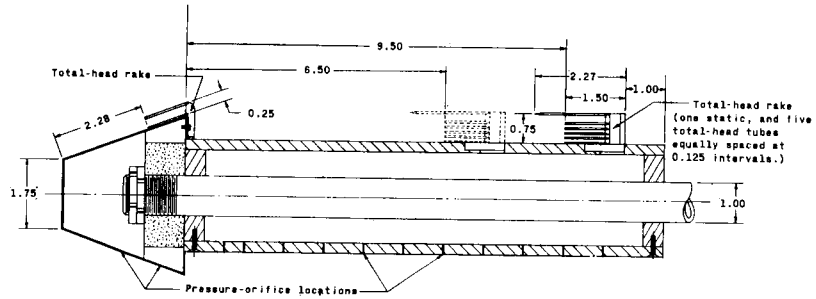

(a) Pressure configuration.

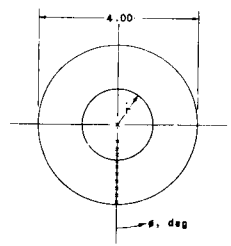

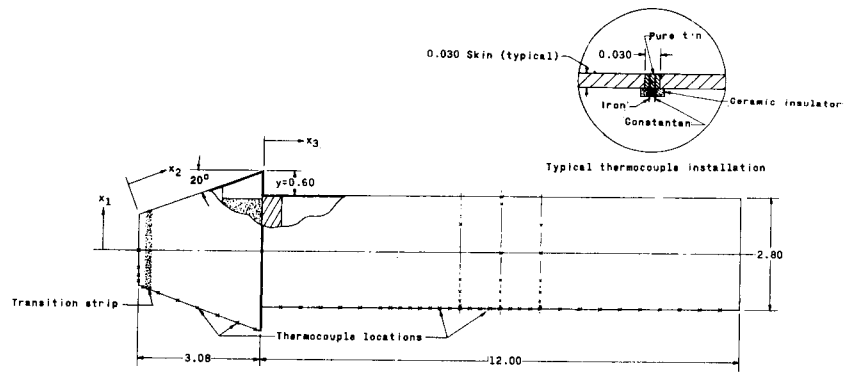

(b) Heat-transfer configuration.

Figure 1.- Details of stepped-cylinder model with thermocouple and pressure-orifice locations. (All dimensions are in inches unless otherwise indicated.)

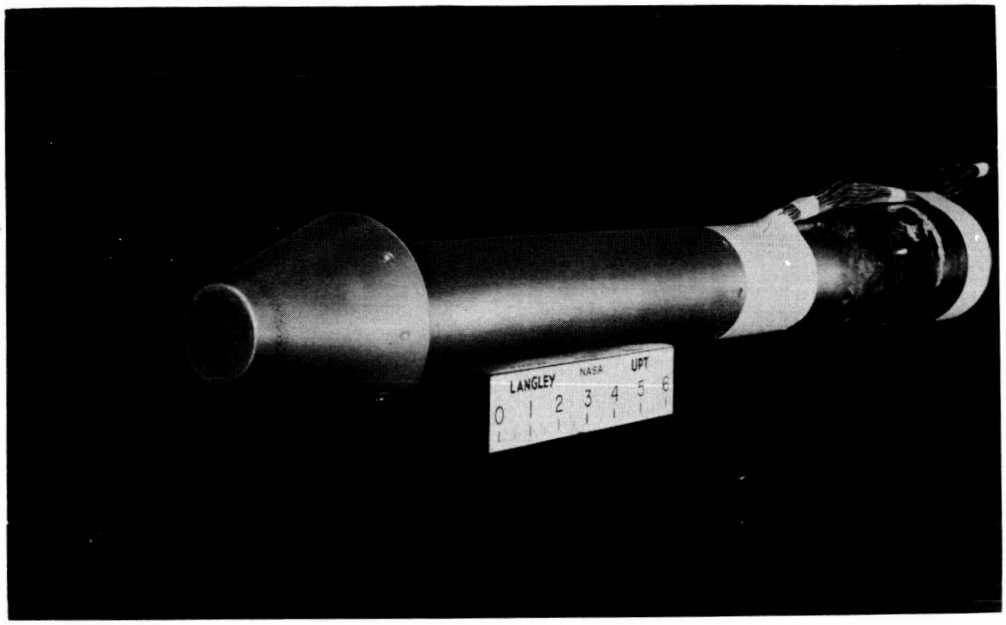

(a) Heat-transfer configuration. L-60-3705

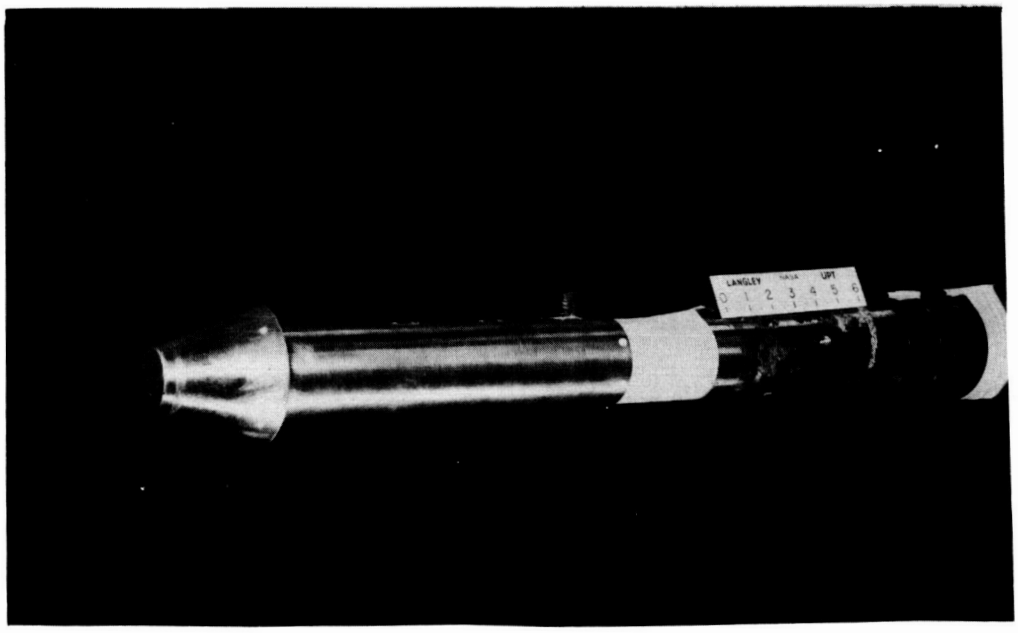

L-60-3702

(b) Pressure configuration with rearward pressure rake installed.

Figure 2.- Stepped-cylinder model.

Thermo-couple	Skin thickness, b, in.	Meridian angle, ø, deg	x, in.
1	0.0250	0	58.98
2	.0250	0	59.98
3	.0250	0	60.98
4	.0250	180	58.98
5	.0250	180	59.98
6	.0250	180	60.98
7	.0330	0	75.08
8	.0330	0	76.08
9	.0330	0	77.08
10	.0330	0	78.08
11	.0330	0	79.08
12	.0310	0	80.28
13	.0310	0	80.48
14	.0310	0	80.68
15	.0310	0	80.88
16	.0300	0	81.33
17	.0300	0	81.58
18	.0300	0	81.83
19	.0310	0	82.08
20	.0310	0	82.33
21	.0310	0	82.58
22	.0310	0	82.83
23	.0310	0	83.08
24	.0310	0	83.33
25	.0310	0	83.58
26	.0310	0	83.83
27	.0310	0	84.08
28	.0310	0	84.33
29	.0310	0	84.58
30	.0310	0	84.83
31	.0310	0	85.08
32	.0320	0	85.33
33	.0320	0	85.58
34	.0310	0	85.83
35	.0300	180	80.28
36	.0310	180	80.48
37	.0310	180	80.68
38	.0310	180	80.88
39	.0310	180	81.33
40	.0310	180	81.58
41	.0310	180	81.83
42	.0310	180	82.08
43	.0310	180	82.33
44	.0310	180	82.58
45	.0310	180	82.83
46	.0310	180	83.08
47	.0310	180	83.33
48	.0310	180	83.58
49	.0310	180	83.83
50	.0310	180	84.08
51	.0310	180	84.33
52	.0310	180	84.58
53	.0310	180	84.83
54	.0310	180	85.08
55	.0310	180	85.33
56	.0310	180	85.58
57	.0310	180	85.83

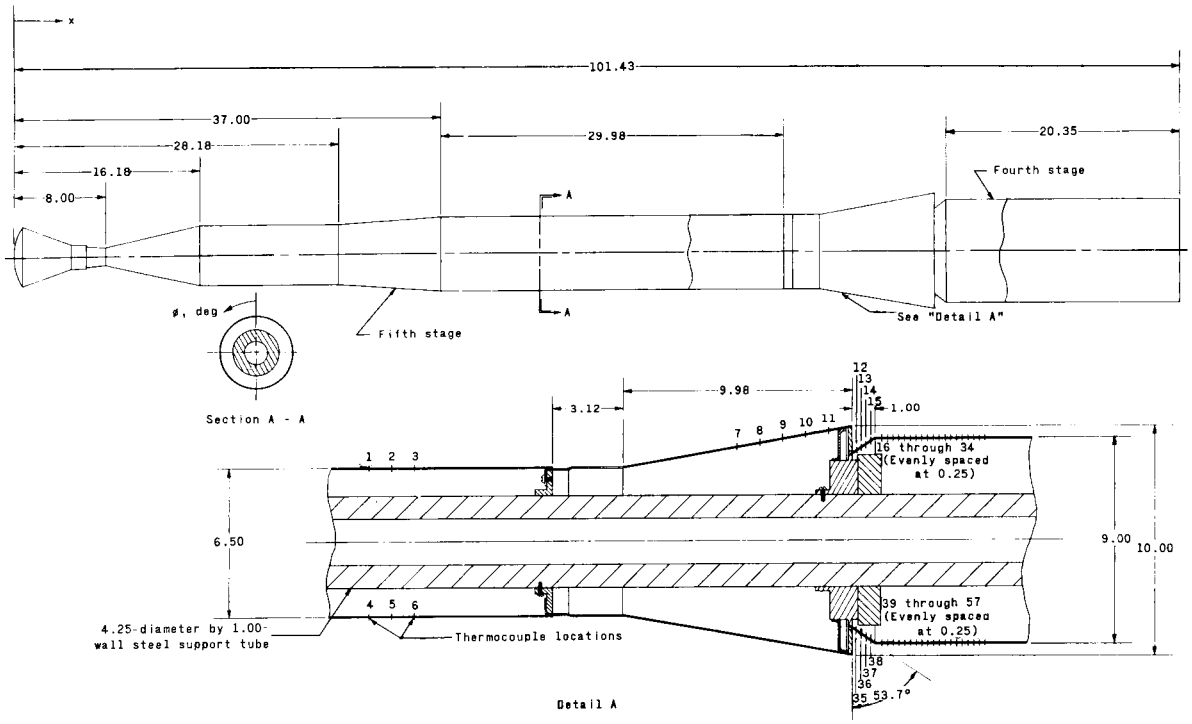

Figure 3.- Details of five-stage research vehicle model with thermocouple locations. (All dimensions are in inches unless otherwise indicated.)

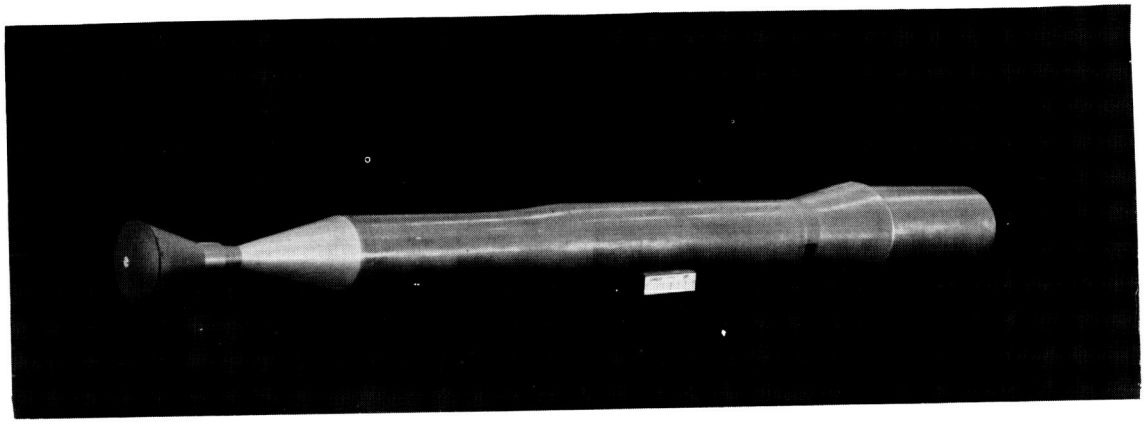

(a) Complete model. L-60-4615

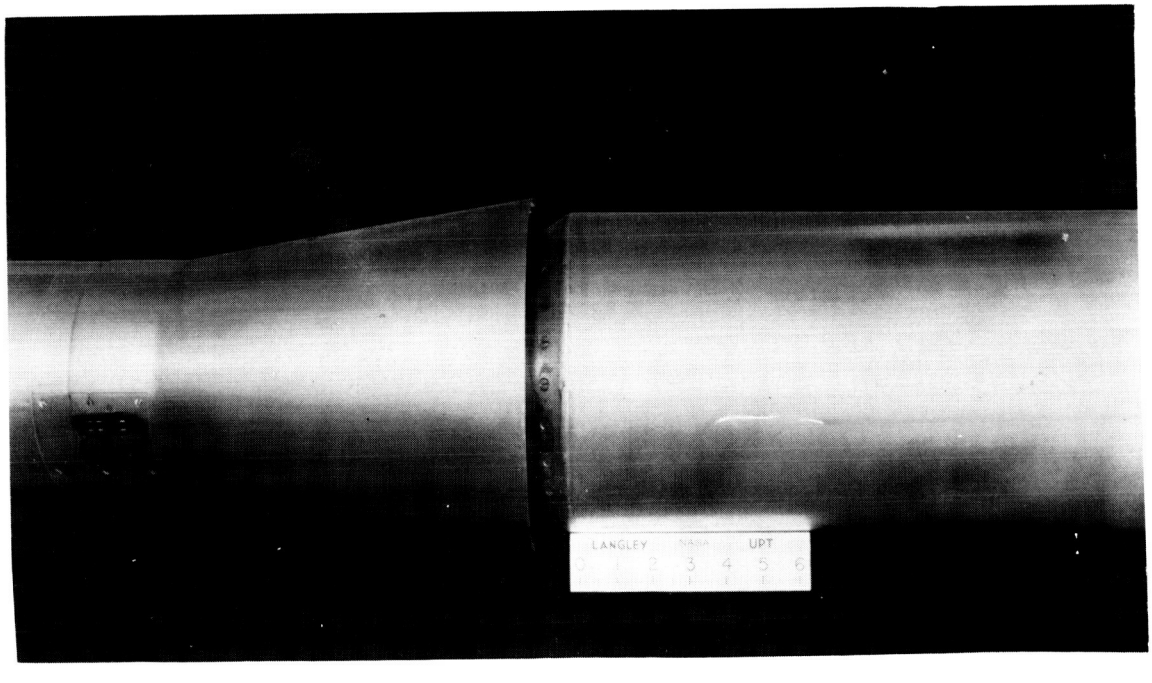

(b) Enlargement of step. L-60-4617

Figure 4.- Five-stage research vehicle model.

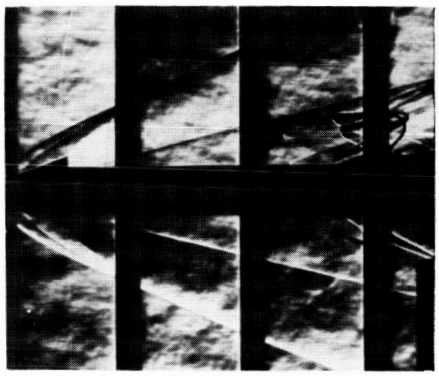

α = 0°

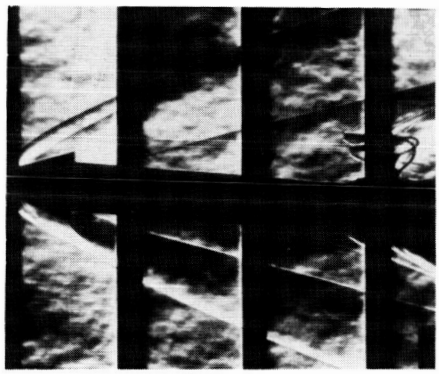

α = 5°

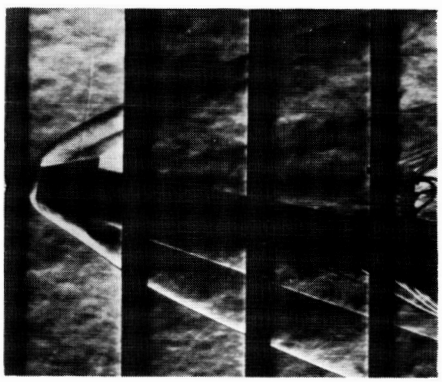

α = 10°

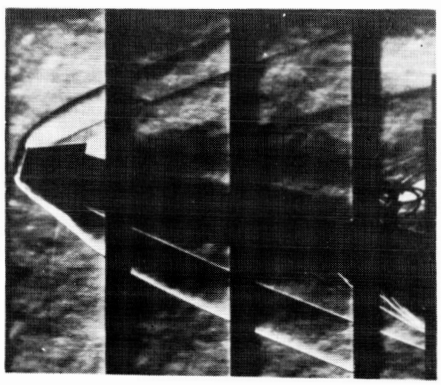

α = 15°

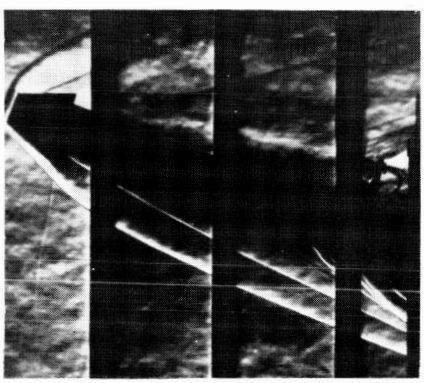

α = 20°

(a) M = 2.65; R = 3.1×10^6. L-61-2193

Figure 5.- Typical schlieren photographs of stepped-cylinder model.

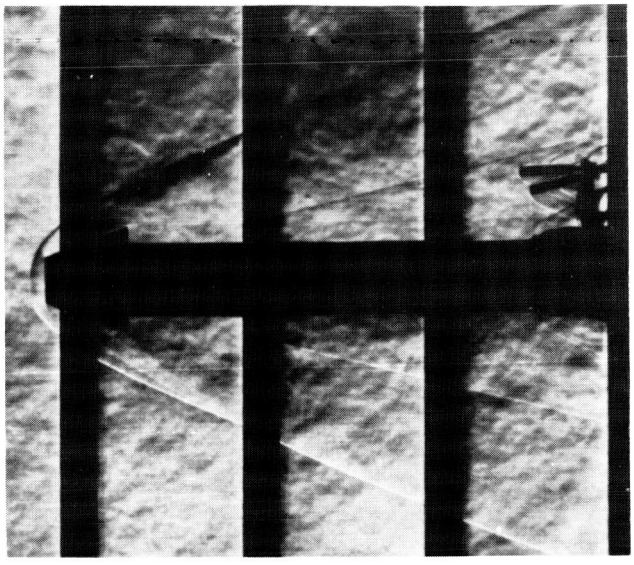

α = 0°

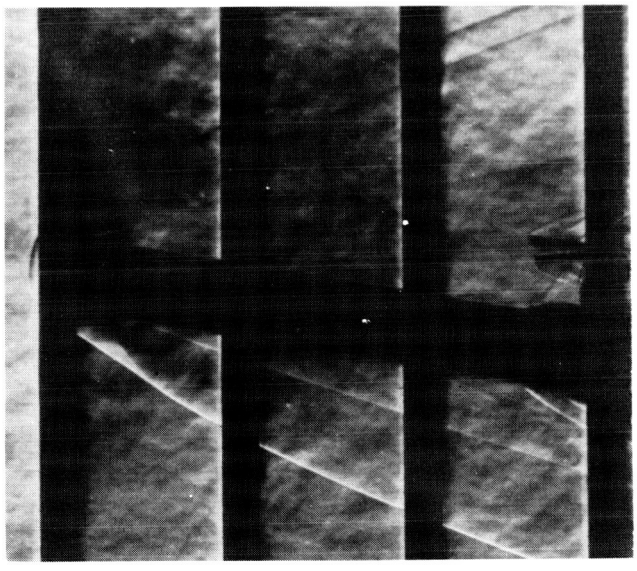

α = 10°

(b) M = 3.51; R = 1.0×10^6. L-61-2192

Figure 5.- Continued.

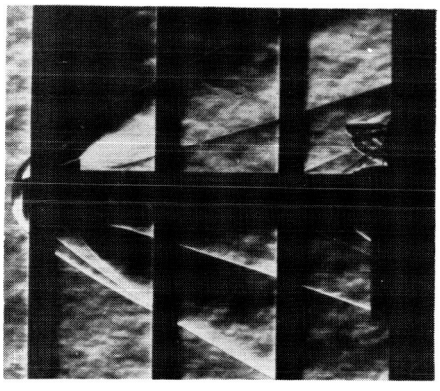

$\alpha = 0°$

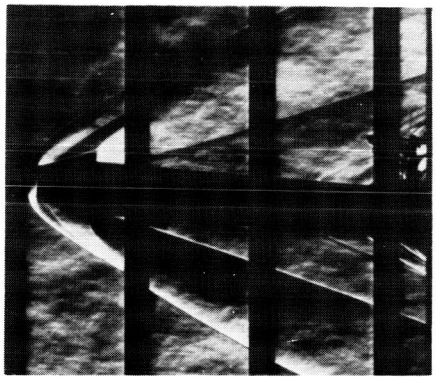

$\alpha = 5°$

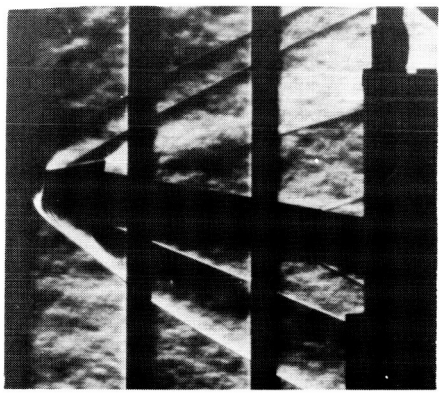

$\alpha = 10°$

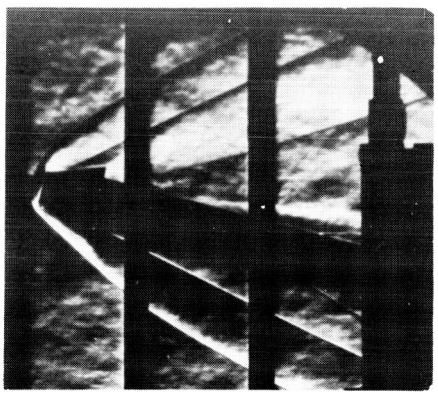

$\alpha = 15°$

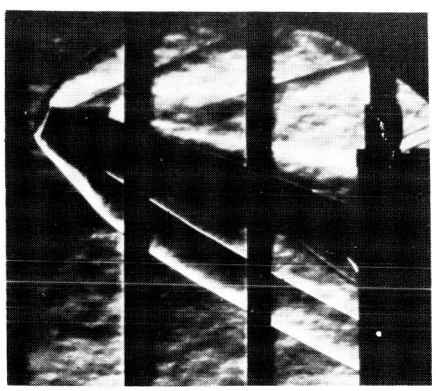

$\alpha = 20°$

(c) $M = 3.51$; $R = 3.5 \times 10^6$. L-61-2191

Figure 5.- Concluded.

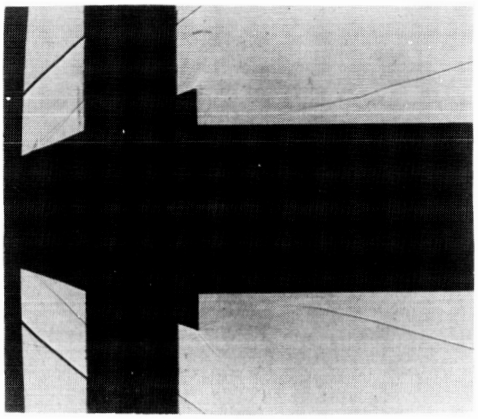

α = 0°

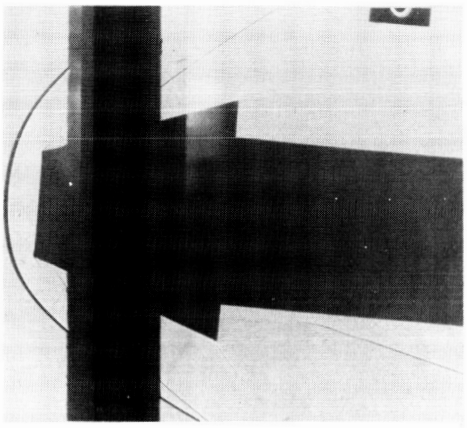

α = 5°

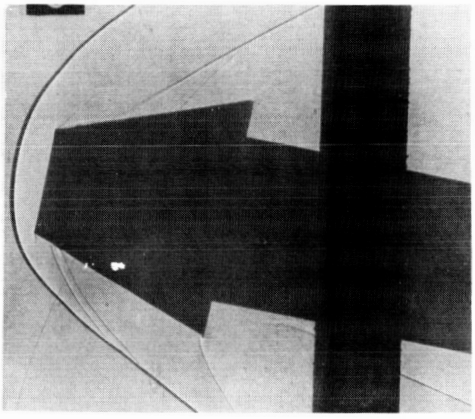

α = 10°

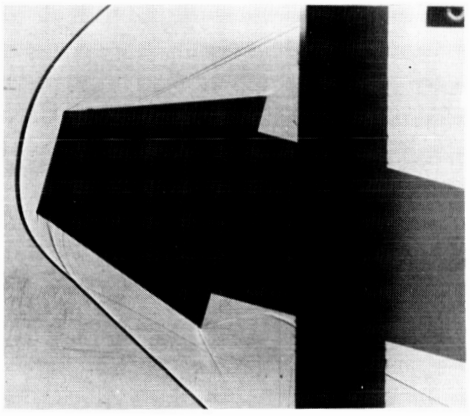

α = 15°

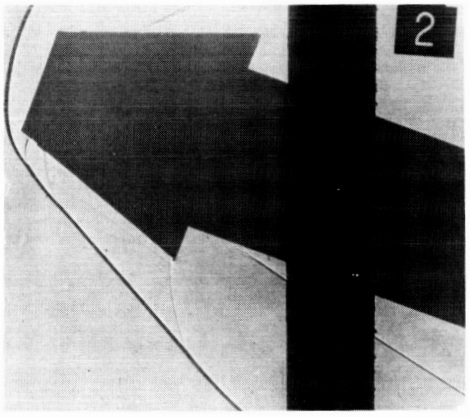

α = 20°

(a) M = 2.65; R = 3.1×10^6. L-61-2194

Figure 6.- Typical shadowgraph photographs of stepped-cylinder model.

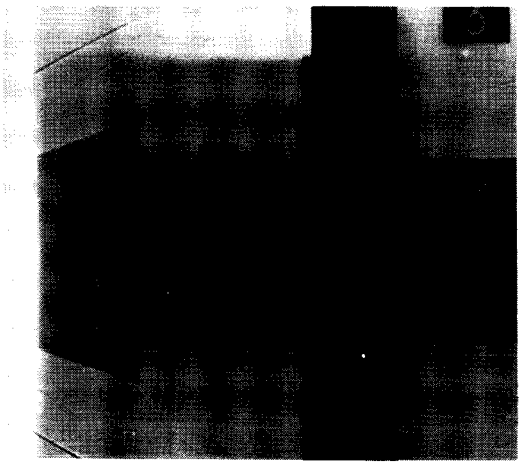

α = 0°

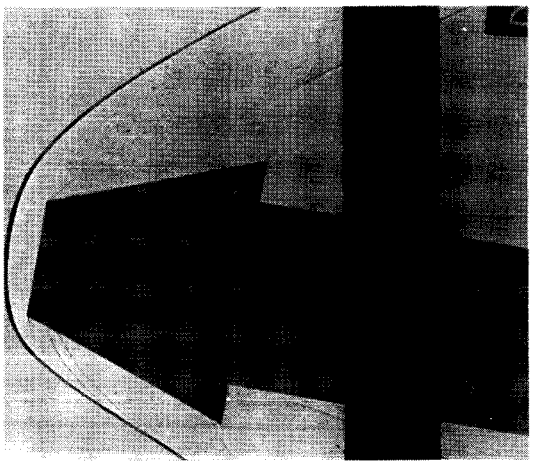

α = 10°

α = 20°

(b) M = 3.51; R = 3.5×10^6. L-61-2195

Figure 6.- Concluded.

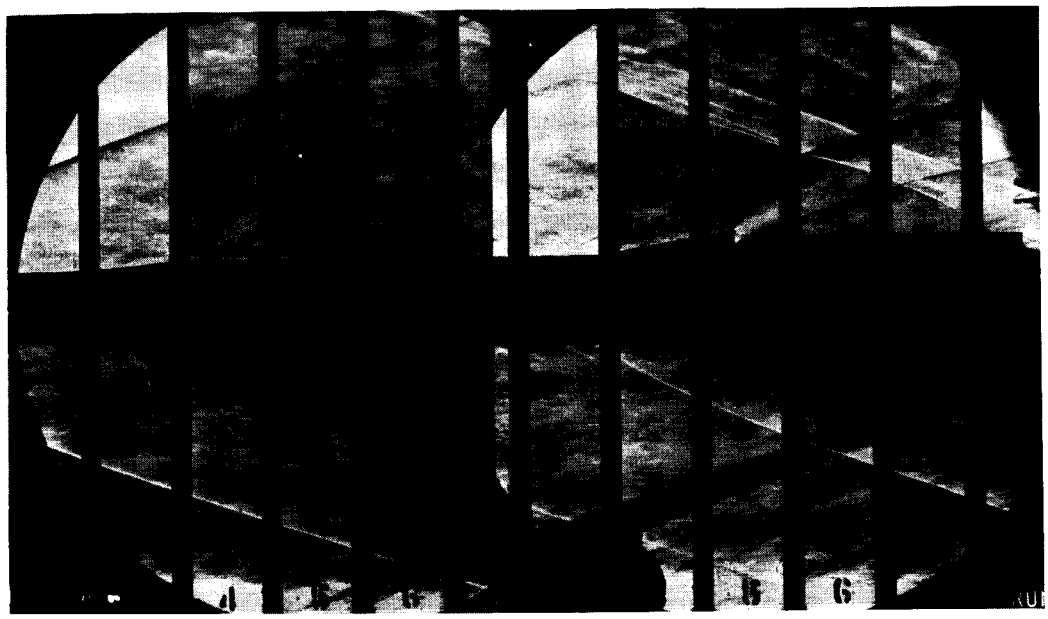

(a) M = 3.51; R = 2.2×10^6.

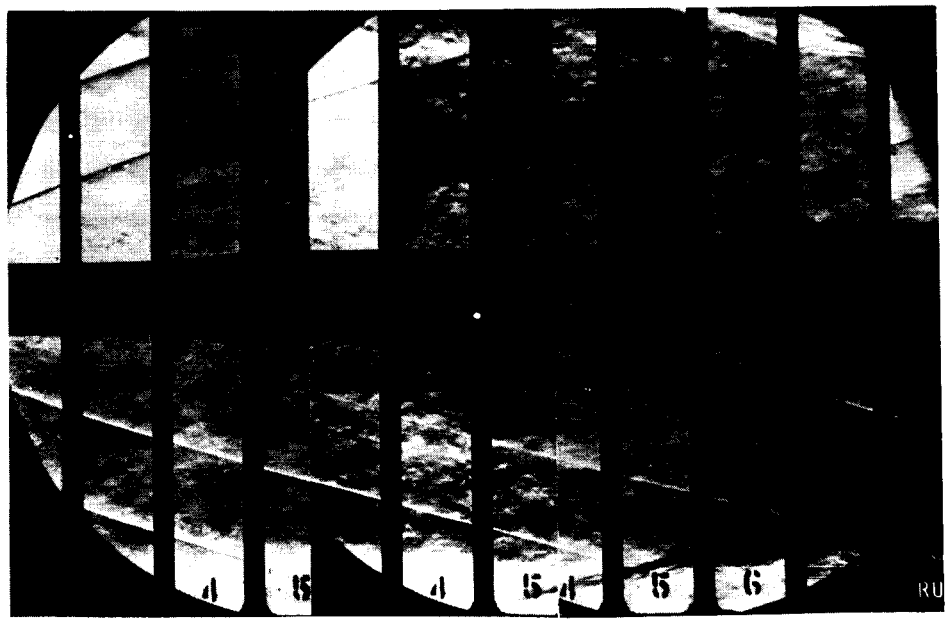

(b) M = 4.50; R = 3.2×10^6. L-61-2196

Figure 7.- Composite schlieren photographs of five-stage research vehicle model. $\alpha = 0^\circ$.

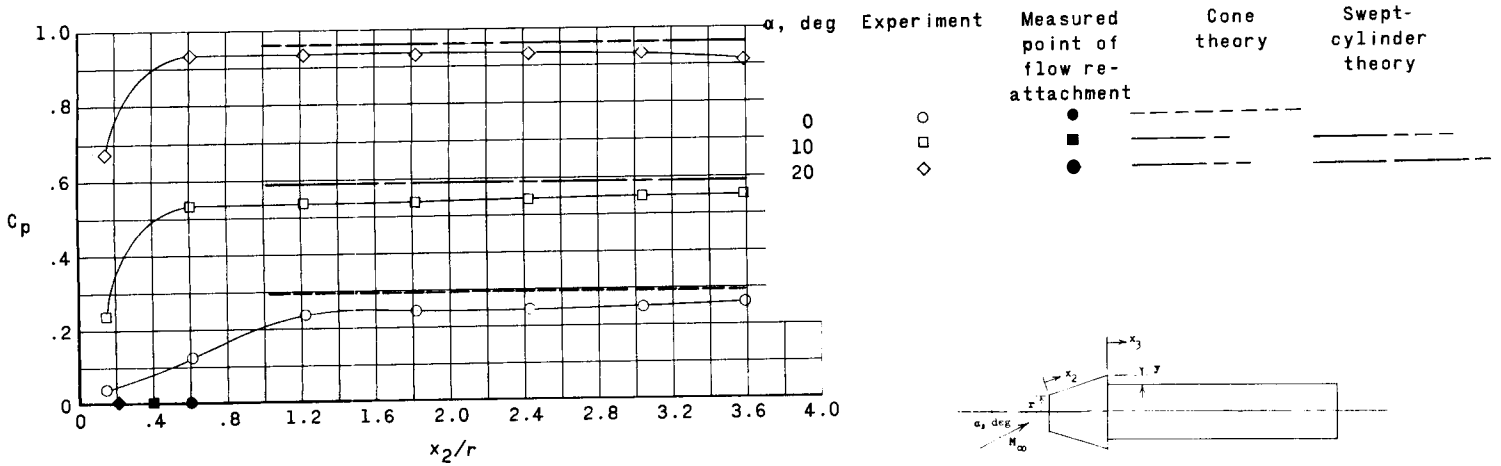

(a) Conical portion of nose.

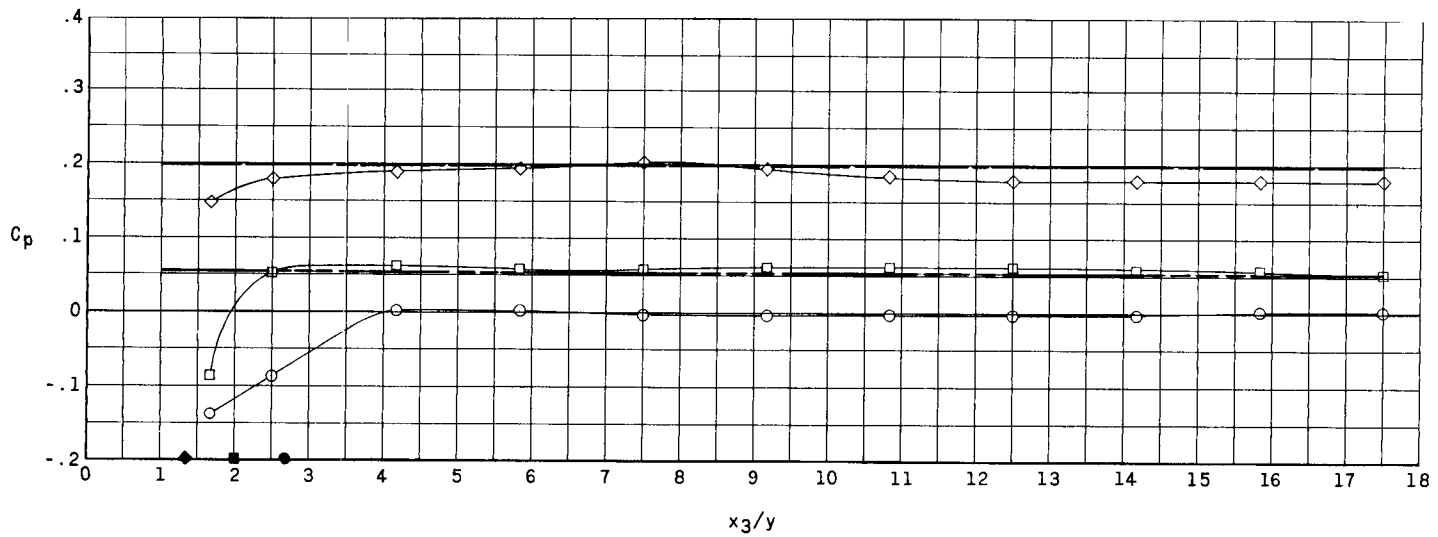

(b) Cylindrical afterbody.

Figure 8.- Effect of angle of attack on pressure-coefficient distribution along windward meridian of stepped-cylinder model. M = 2.65; R = 3.1×10^6.

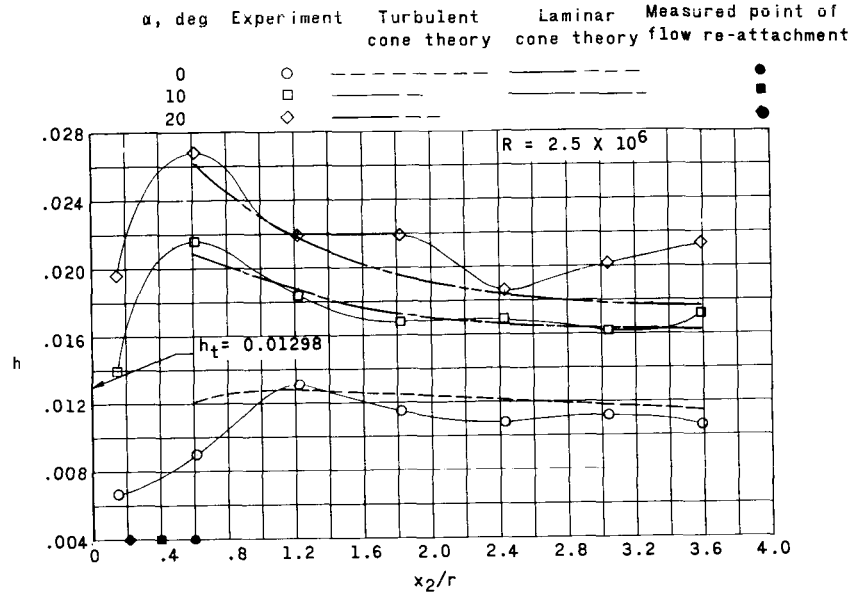

(a) M = 2.65.

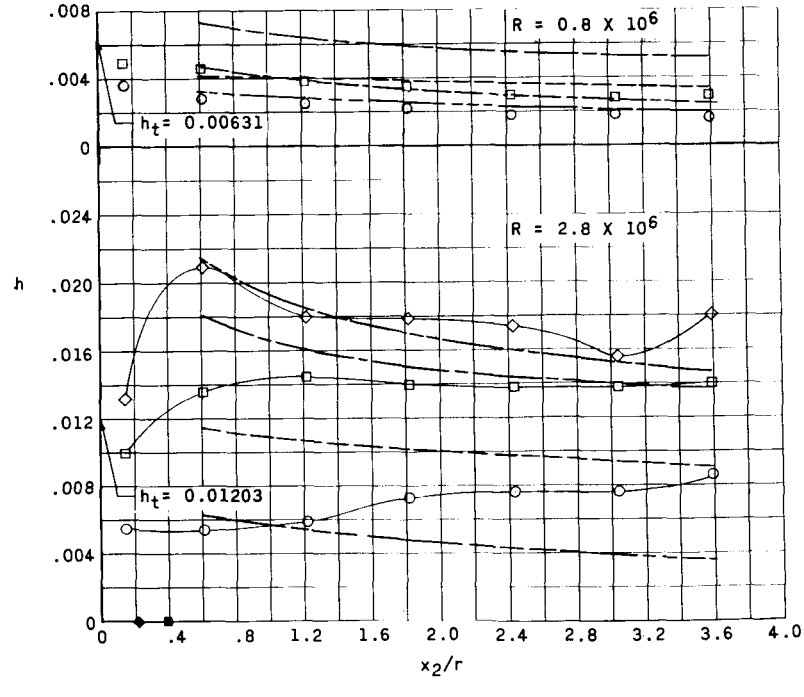

(b) M = 3.51.

Figure 9.- The effect of angle of attack, Mach number, and Reynolds number on local heat-transfer-coefficient distribution along windward meridian of conical nose of stepped-cylinder model.

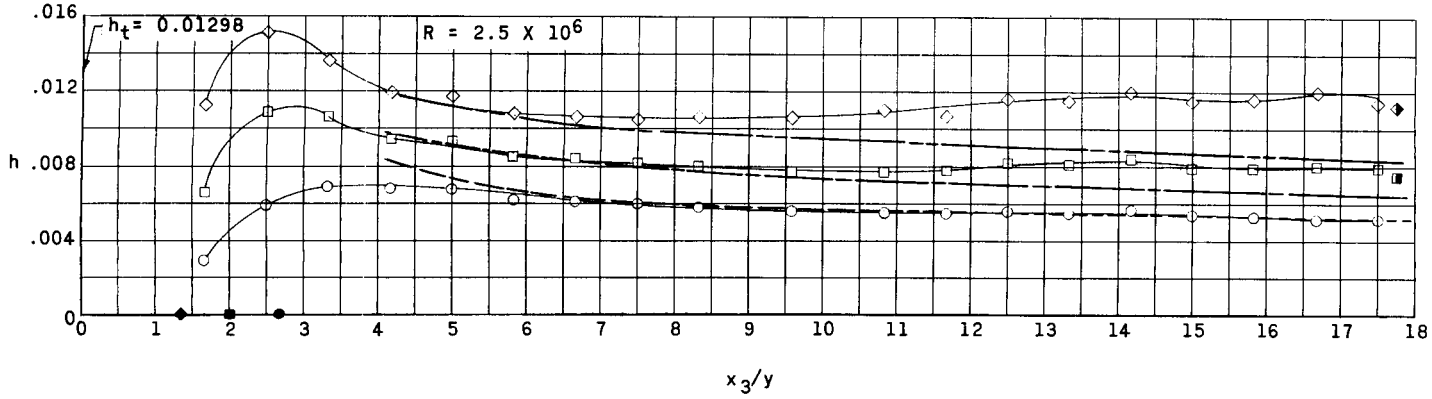

(a) M = 2.65.

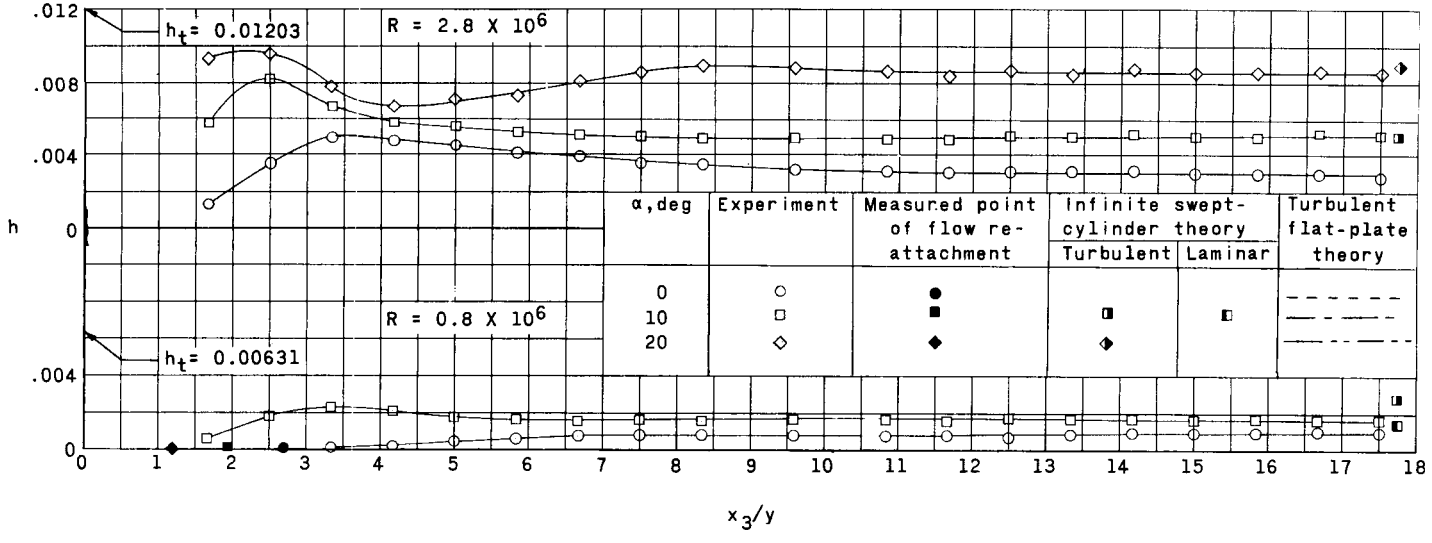

(b) M = 3.51.

Figure 10.- The effect of angle of attack, Mach number, and Reynolds number on local heat-transfer-coefficient distribution along windward meridian of afterbody of stepped-cylinder model.

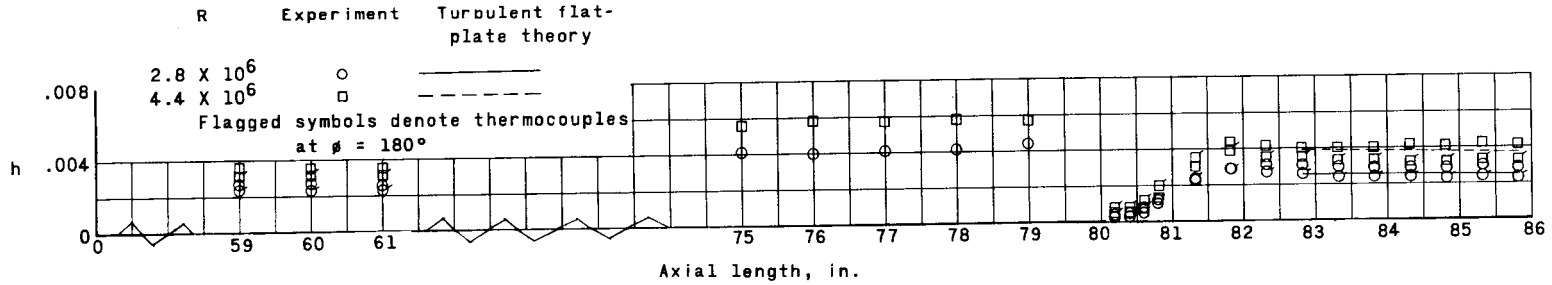

(a) M = 3.51.

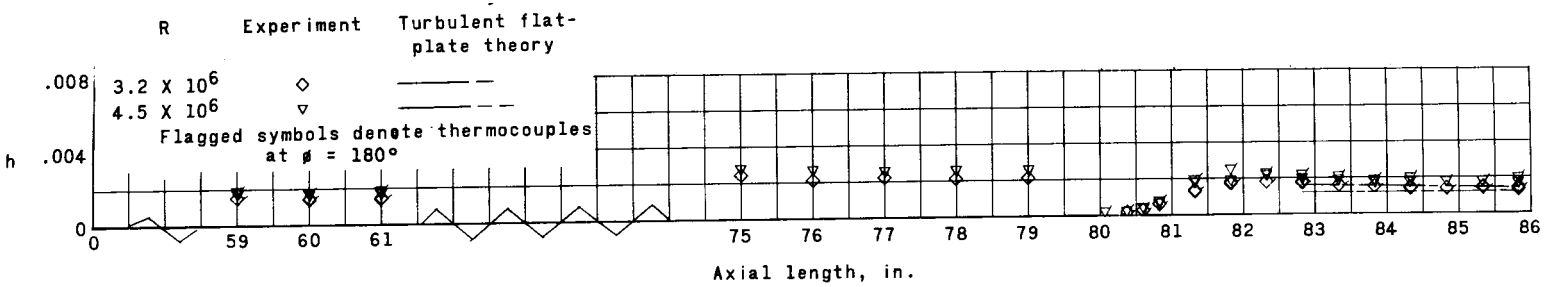

(b) M = 4.50.

Figure 11.- The effect of Mach number and Reynolds number on the heat-transfer-coefficient distribution measured on the five-stage research vehicle model. $\alpha = 0^{\circ}$.